NAVAL POSTGRADUATE SCHOOL

MONTEREY, CALIFORNIA

THESIS

CARBON NANOFIBER WIRING STRUCTURE WITHIN A MICROBIAL FUEL CELL DEVICE

by

Analise M. Marshall

September 2023

Thesis Advisor:	Emil P. Kartalov
Second Reader:	Dragoslav Grbovic

THIS PAGE INTENTIONALLY LEFT BLANK

REPORT DOCUMENTATION PAGE	*Form Approved OMB No. 0704-0188*

1. AGENCY USE ONLY *(Leave blank)*	**2. REPORT DATE** September 2023	**3. REPORT TYPE AND DATES COVERED** Master's thesis

4. TITLE AND SUBTITLE
CARBON NANOFIBER WIRING STRUCTURE WITHIN A MICROBIAL FUEL CELL DEVICE

5. FUNDING NUMBERS

6. AUTHOR(S) Analise M. Marshall

7. PERFORMING ORGANIZATION NAME(S) AND ADDRESS(ES)
Naval Postgraduate School
Monterey, CA 93943-5000

8. PERFORMING ORGANIZATION REPORT NUMBER

9. SPONSORING / MONITORING AGENCY NAME(S) AND ADDRESS(ES)
N/A

10. SPONSORING / MONITORING AGENCY REPORT NUMBER

11. SUPPLEMENTARY NOTES The views expressed in this thesis are those of the author and do not reflect the official policy or position of the Department of Defense or the U.S. Government.

12a. DISTRIBUTION / AVAILABILITY STATEMENT
Approved for public release. Distribution is unlimited.

12b. DISTRIBUTION CODE
A

13. ABSTRACT (maximum 200 words)

The Navy 30-year Science and Technology Strategic Plan heavily emphasizes investment in unmanned underwater vehicles (UUVs). These assets are becoming strategically significant and essential within the realm of undersea warfare. This proposed project aims to continue the development of biofuel cells, which are critical for the logistics of undersea assets. Biofuel cells would provide a robust, resilient distributed network of renewable-power stations. The alternatives for an undersea warfare power source are batteries, which would deplete quickly, or the use of capital ships which would be an inefficient use of key assets.

Benthic bacteria are known to produce electrons as waste which can be harvested for remote power. These organisms are naturally occurring in marine sediment and are effectively self-sustaining in the devices in which they are exploited. Previous proof of concept work has shown a two-dimensional H-fractal architecture to produce on the order of 80 milliwatts per meter squared, four times the amount of previous benthic microfluidic designs. The two-dimensional design serves as the groundwork for scalable three-dimensional units.

Scaling to three-dimensions offers a path to strategically placed power cubes in an ocean environment, but not without manufacturing hurdles. Thesis work will include solving known problems in 3D printing to create stackable biofuel cells and will seek to prove superior power density within the existing channel designs.

14. SUBJECT TERMS microbial fuel cell, benthic microbial fuel cell, microfluidics, microelectrode	**15. NUMBER OF PAGES** 65
	16. PRICE CODE

17. SECURITY CLASSIFICATION OF REPORT	**18. SECURITY CLASSIFICATION OF THIS PAGE**	**19. SECURITY CLASSIFICATION OF ABSTRACT**	**20. LIMITATION OF ABSTRACT**
Unclassified	Unclassified	Unclassified	UU

NSN 7540-01-280-5500

Standard Form 298 (Rev. 2-89)
Prescribed by ANSI Std. 239-18

THIS PAGE INTENTIONALLY LEFT BLANK

Approved for public release. Distribution is unlimited.

CARBON NANOFIBER WIRING STRUCTURE WITHIN A MICROBIAL FUEL CELL DEVICE

Analise M. Marshall
Lieutenant, United States Navy
BS, University of Colorado, Denver, 2016

Submitted in partial fulfillment of the
requirements for the degree of

MASTER OF SCIENCE IN APPLIED PHYSICS

from the

NAVAL POSTGRADUATE SCHOOL
September 2023

Approved by: Emil P. Kartalov
Advisor

Dragoslav Grbovic
Second Reader

Frank A. Narducci
Chair, Department of Physics

THIS PAGE INTENTIONALLY LEFT BLANK

ABSTRACT

The Navy 30-year Science and Technology Strategic Plan heavily emphasizes investment in unmanned underwater vehicles (UUVs). These assets are becoming strategically significant and essential within the realm of undersea warfare. This proposed project aims to continue the development of biofuel cells, which are critical for the logistics of undersea assets. Biofuel cells would provide a robust, resilient distributed network of renewable-power stations. The alternatives for an undersea warfare power source are batteries, which would deplete quickly, or the use of capital ships which would be an inefficient use of key assets.

Benthic bacteria are known to produce electrons as waste which can be harvested for remote power. These organisms are naturally occurring in marine sediment and are effectively self-sustaining in the devices in which they are exploited. Previous proof of concept work has shown a two-dimensional H-fractal architecture to produce on the order of 80 milliwatts per meter squared, four times the amount of previous benthic microfluidic designs. The two-dimensional design serves as the groundwork for scalable three-dimensional units.

Scaling to three-dimensions offers a path to strategically placed power cubes in an ocean environment, but not without manufacturing hurdles. Thesis work will include solving known problems in 3D printing to create stackable biofuel cells and will seek to prove superior power density within the existing channel designs.

THIS PAGE INTENTIONALLY LEFT BLANK

Table of Contents

1 Introduction **1**

1.1 Microbial Fuel Cells 1

1.2 Naval Applications 4

1.3 Current MFC Progress 5

1.4 Carbon Nanofibers 10

2 Experimental Methodology **11**

2.1 Channel Design Concepts in 2022. 11

2.2 Chip Processing Procedures and Methods. 14

3 Results **21**

3.1 Mass Loss Outgassing 21

3.2 Custom Resin Resistances 22

3.3 T-Channel Resistances After Dry-Cycling with CNF in Isopropyl Alcohol . . 24

3.4 Square Channel Resistances After Dry-Cycling with CNF in Isopropyl Alcohol 25

4 Discussion **37**

4.1 Mass Loss Outgassing, Custom Resins, and T-Channel Resistances 37

4.2 Soft Square Channels. 38

4.3 Hard Square Channels 40

4.4 Future Work 41

5 Conclusion **43**

List of References **45**

Initial Distribution List **49**

THIS PAGE INTENTIONALLY LEFT BLANK

List of Figures

Figure 1.1 A typical two-chamber MFC. 2

Figure 1.2 A typical BMFC. 3

Figure 1.3 U.S. Navy 30 Year Plan Illustration. 5

Figure 1.4 Assembled microfluidic MFC chip. 8

Figure 1.5 H-architecture MFC depiction. 8

Figure 1.6 Top view of microfluidic dome template. 9

Figure 2.1 Concept depiction of the T-channel architecture. 12

Figure 2.2 Illustration of T-channel dimensions. 12

Figure 2.3 Freshly printed chip example. 14

Figure 2.4 Frontal view of a printed chip. 15

Figure 2.5 Specific CNFs used in custom solutions. 17

Figure 2.6 Custom resin PCB preparation. 18

Figure 2.7 Soft square channel examples. 20

Figure 2.8 Hard square channel example. 20

Figure 3.1 Mass loss outgassing histogram. 22

Figure 3.2 Plot of graphene custom resin conductivities. 23

Figure 3.3 Plot of carbon mesoporous custom resin conductivities. 23

Figure 3.4 Plot of carbon nanofiber custom resin conductivities. 24

Figure 3.5 T-channel resistance plot. 25

Figure 3.6 600 micron soft channel resistance plot. 26

Figure 3.7 720 micron soft channel resistance plot. 27

Figure 3.8 840 micron soft channel resistance plot. 27
Figure 3.9 960 micron soft channel resistance plot. 28
Figure 3.10 1080 micron soft channel resistance plot. 28
Figure 3.11 600 micron soft channel averages. 29
Figure 3.12 720 micron soft channel averages. 29
Figure 3.13 840 micron soft channel averages. 30
Figure 3.14 960 micron soft channel averages. 30
Figure 3.15 1080 micron soft channel averages. 31
Figure 3.16 Soft channel compiled averages. 31
Figure 3.17 Channel darkening images after dry-cycling. 32
Figure 3.18 512 micron hard channel resistance plot. 33
Figure 3.19 608 micron hard channel resistance plot. 33
Figure 3.20 764 micron hard channel resistance plot. 34
Figure 3.21 896 micron hard channel resistance plot. 34
Figure 3.22 996 micron hard channel resistance plot. 35

List of Tables

Table 2.1 Clearance procedure. 15

Table 2.2 Wiring procedure. 19

THIS PAGE INTENTIONALLY LEFT BLANK

List of Acronyms and Abbreviations

2D	Two-dimensional
3D	Three-dimensional
BMFC	Benthic Microbial Fuel Cell
CNF	Carbon Nanofiber
CNT	Carbon Nanotube
MFC	Microbial Fuel Cell
NaOH	Sodium Hydroxide
NPS	Naval Postgraduate School
PCB	Printed Circuit Board
PDMS	Polydimethylsiloxane
UV	Ultraviolet

THIS PAGE INTENTIONALLY LEFT BLANK

CHAPTER 1:
Introduction

The U.S. Navy's 30-year Shipbuilding Plan [1] and the Chief of Naval Operations 2022 Navigation Plan [2] reflect an increased investment in unmanned sensors and underwater vehicles. Both play a substantive role in expanding the distribution of forces geographically to gain an advantage over an adversary. These assets promise to cover larger areas of interest to expand the intelligence, reconnaissance, and surveillance footings of the United States [2]. With an unmanned capacity goal of approximately 150 vessels, the survivability and cost effectiveness of the fleet will be greatly improved [2]. However, powering these assets stands as a logistical challenge with regard to stealth and mission effectiveness. The supply lines of petroleum, natural gas, and coal are susceptible to geopolitical crises and their use runs counter to the Navy's clean energy initiative [3]. A solution to this energy problem is a local network of power stations offering a renewable source of power; benthic microbial fuel cells could be this source of renewable power [4].

1.1 Microbial Fuel Cells

A fuel cell is a source of power that is similar to a battery. It converts the chemical energy released by a reaction to electrical power through the presence of two electrodes: an anode and a cathode. The anode oxidizes the fuel while the cathode reduces the oxidant [4]. A fuel cell differs from a battery in that it does not store its reactants and products internally, but rather receives reactants and removes products externally. In other words, a fuel cell can be a source of long-term power generation as long as fuel is continuously supplied and waste products are removed [4]. A microbial fuel cell (MFC) is an electrochemical system in which microorganisms are used to convert chemical energy into electrical power [5]. As described in [4] and [6], in a traditional MFC the cathode and anode are separated at a junction consisting of a membrane with a slurry of organic matter present for fuel at the anode. Anaerobic bacteria oxidize the organic matter at the anode to produce electrons and protons. Electricity can be generated and harvested for remote power by making an electrical connection between the anode and the cathode. The expelled "waste charge" is conducted through the device to be powered and arrives at the cathode, where the electrons

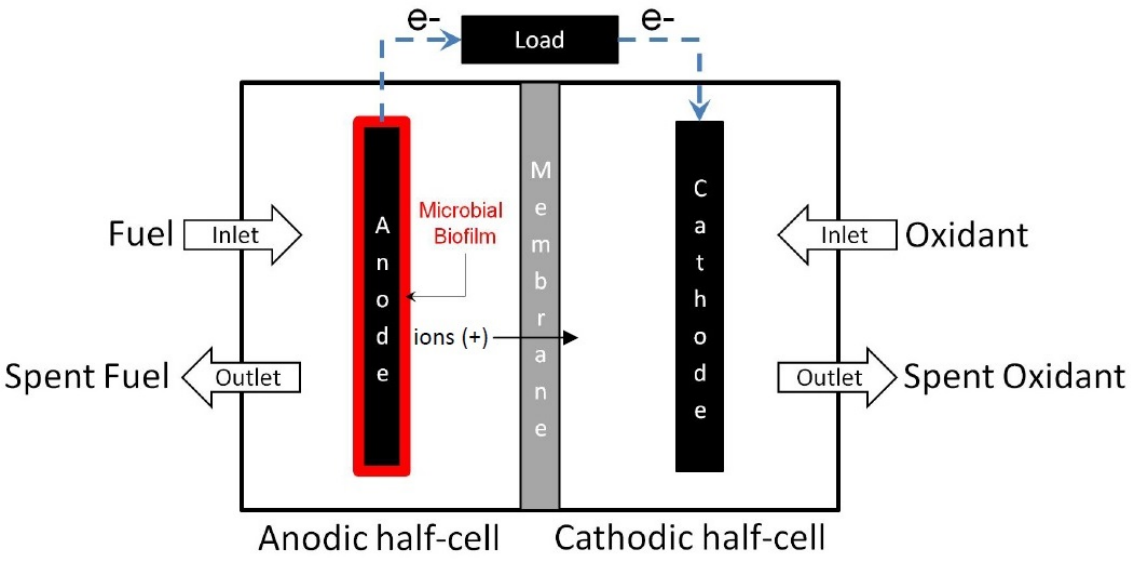

Figure 1.1. A schematic of a typical two-chamber MFC with traditional membrane. Source: [4]

are consumed through reduction [4], [6].

1.1.1 Benthic Microbial Fuel Cells

The organisms capable of performing the biological processes necessary to produce electrons are naturally occurring in marine sediment. The most important for the purposes of MFCs are known as benthic bacteria. Many sources [6]–[10] provide in-depth background regarding these benthic bacteria and their discussions can be summarized succinctly. Benthic bacteria reside in the benthic zone (the lowest ecological region of a body of water, in other words, the seafloor). Their populations are large and on the order of billions in a single teaspoon of sediment. When specifically benthic bacteria are used in a MFC on the seafloor, the device becomes a benthic microbial fuel cell (BMFC). The design of a BMFC is nearly identical to a traditional MFC, with the main difference being the incorporation of marine sediment and/or the seafloor directly into the fuel cell's makeup. The seawater/seafloor interface acts as the ion exchange membrane. The seafloor hosts the anode and the seawater above hosts the cathode. The benthic bacteria present in the seafloor oxidize organic matter found in sediment pore water which acts as fuel in the fuel cell. This organic matter is extremely plentiful. It generally consists of dead phytoplankton that fall from the ocean

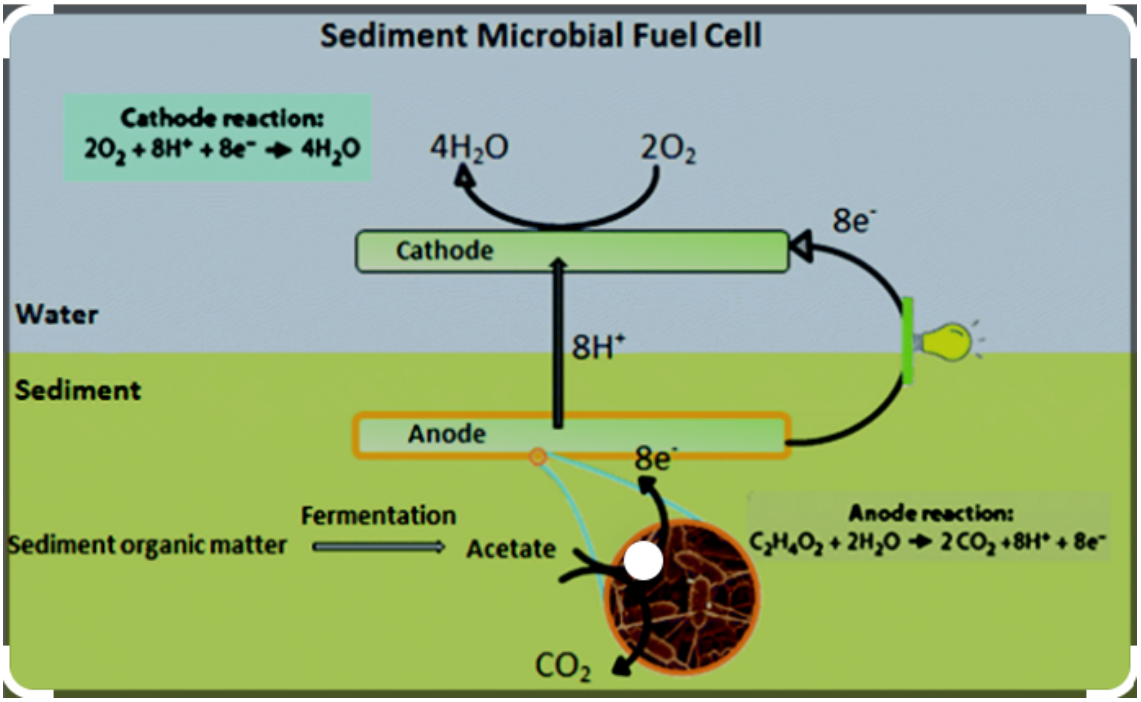

Figure 1.2. A schematic of a typical BMFC oriented in marine sediment. Source: [11]

water above and accumulate on the seabed in the sediment layer. Oxygen in the seawater above the sediment layer acts as the oxidant in the fuel cell [6]–[10]. The cathode and anode typically are manufactured from graphite or a carbon-based material due to their electrical and pro-microbial properties [4].

Currently, BMFCs are the only microbial fuel cell known to produce a net positive power output and are therefore being investigated as a source of long term, renewable underwater power [4]. Their advantages include: 1) endurance i.e. continue to feed the bacteria and remove their waste products and they will produce charge indefinitely); 2) natural processes i.e. the specialized catalysts and membranes required in a conventional fuel cell are no longer required as the bacteria already undergo these biologic, catalytic processes through their normal life cycles; 3) low cost due to the second advantage [4], [5]. But there are drawbacks to BMFCS, too. While the use of external catalysts is eliminated, the catalytic rate the bacteria offer as a replacement is orders of magnitude slower [7]. As a result, BMFC power density suffers and is relatively low in comparison to its conventional counterpart.

Improving power density is the key point of interest in current BMFC design. Fuel cell geometry, mass transport rate, electrode and fuel cell materials, etc. are all thought to play a role in BMFC performance [10]. Thus, novel designs for BMFCs are of keen interest to the Navy.

1.2 Naval Applications

Distributed networks for communications and sensors are vital to the future of sea power. This concept can be applied to networks of charging stations necessary to power certain types of propulsion, sensors, acoustic networks, surveillance systems, environmental monitoring, navigation systems, etc. BMFC technology is easily employed here.

A current drawback of the forward operation of remote sensors and vehicles is their delivery to the area of operation. Ships, submarines, and aircraft have the capability to support such systems with their operating, energy, and delivery needs, but these platforms have their own mission sets. Tending to remote equipment is a tedious distraction from what capital ships and warfighting vessels were built and used for. Outfitting remote equipment with the ability to fuel on station eliminates this distraction. Once the equipment is out, it can stay out indefinitely barring any system failures separate from its power needs. Additionally, this concept is an advantage in logistics. A system may deplete its batteries in less than a year of operation in most cases. The options are to retire it in place after such a short lifespan or take it offline to replace the batteries and service it. In the case of an underwater vehicle, it depletes battery life in the transit to arrive on station and return to its launch point, a problem exacerbated when there is no external delivery vessel supporting it. These vehicles have an average operating span of 12-24 hours in most cases with a limited range because of this. Installing a network of BMFC power stations anchored to the seafloor in the littorals would eliminate these problems. Sensor networks could be powered for long periods of time without needing intervention for battery replacement. Underwater vehicles could plug into the tethered stations and operate far longer than 12-24 hours, perhaps for weeks or even months. Advantages in stealth exist, too. A vulnerability for certain sensor networks is their location is revealed when they require multiple trips by humans for servicing batteries. BMFC networks are a solution to this problem and offer a “set it and forget it” operating environment. Underwater vehicles have a similar vulnerability when they require constant transit and repeatedly return to a known location to recharge. The

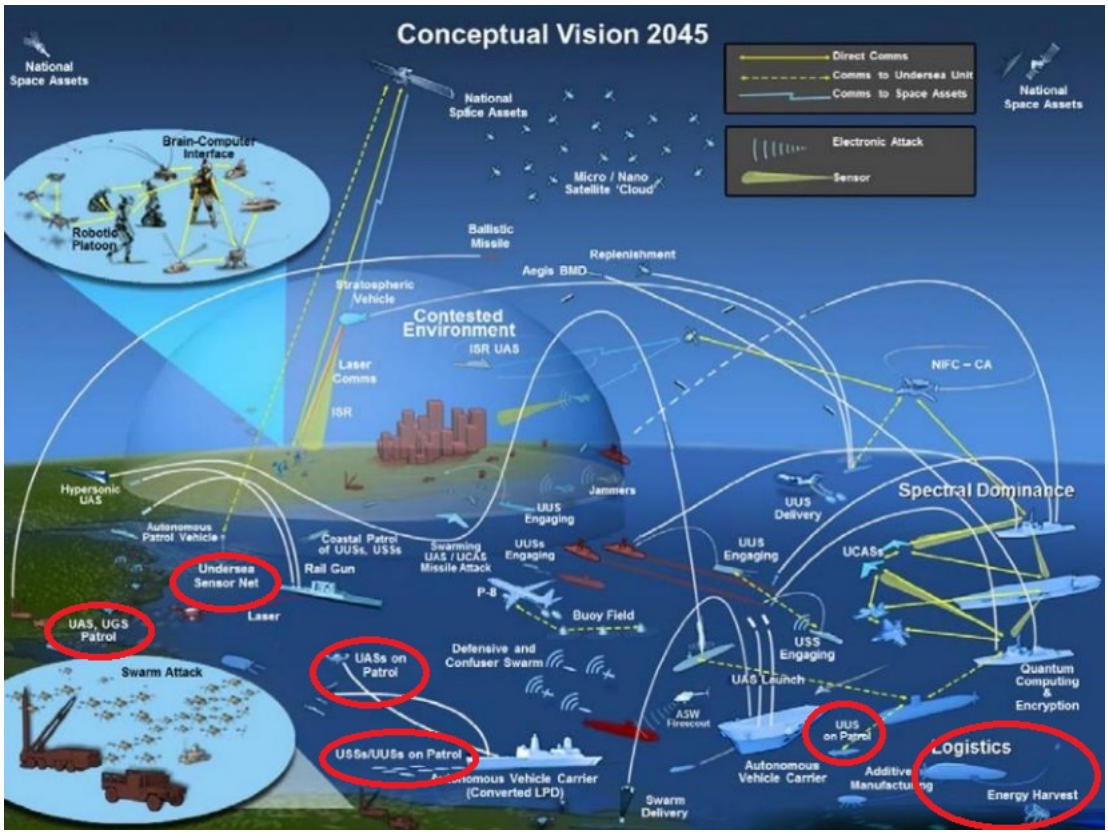

Figure 1.3. Illustration of the role of remote sensors and vehicles from the Navy's 30 Year Plan. Adapted from: [12]

probability of interception is much higher for these vehicles when they are not able to stay in their operating environments for long periods of time.

1.3 Current MFC Progress

Since the potential of BMFC technology became apparent in the early 2000s, the primary goal in investigative research has been to increase their performance. The objective in this global research effort is to develop a BMFC that is scalable with higher power density, has a long lifespan, requires little maintenance, and is able to be used in most underwater environments. Their application goes beyond underwater power and extends to wastewater treatment and bioremediation [13]. As such, much effort and literature has been invested toward BMFCs to address the following problems.

There are some critical issues currently holding BMFCs back as a robust source of remote power. First, their power output is low compared to the energy required for the majority of at-sea equipment. Previous experiments have shown this power density to be on the order of 10-40 mW/m^2 [5], [13]–[15]. This type of power is enough for low and ultra-low power sensors only. To add to this challenge, MFC power capacity does not scale linearly with size [7], [14], [16]–[20]. Even if MFCs could be fabricated on a large scale, simply increasing the biological active surface and making the devices larger has not been shown to boost power output. Some of the devices have been large scale and provided more power density for short periods of time, but their cost inefficiencies along with requiring bulky supplemental equipment tends toward obsolescence. This inability to scale up easily is the most difficult roadblock in BMFC technology, although it is difficult to isolate all factors that may be significant to BMFC performance. Environmental factors and experimental setups i.e. powering different circuits in each study are to blame for this difficulty [7], [16]–[20]. BMFCs are unique as they use natural bacteria and in situ nutrients found in marine sediment and because of this, environmental factors affect performance. Long term sustainment of the benthic bacteria in a BMFC system is a challenge. The bacteria require some feedback controls to optimize their performance. Controlling the environmental pH, temperature, biomass loading, etc. are areas of concern in improving this technology [16].

Several pathways to improvement have already been explored. Current designs have been successful in powering magnetometers [13] and autonomous sensors [14] although with low average output power (10-40 mW/m^2) [5], [13]–[15]. Some studies have modified the anode [21], [22], cathode [23], [24], and both [13], [25], [26] and have shown power density to improve. Others have modified the ocean location of BMFC devices (methane seeps and hydrothermal vents) to achieve power densities on the order of 300-500 mW/m^2 [9], [27]. But this limits the practical deployment of such devices to power naval equipment that is found in all parts of the ocean, not just near methane seeps and hydrothermal vents. Variations in electrode spacing, organic additives such as acetate, and using graphite and carbon-based materials have been shown to raise BMFC performance [16], [18], [22]. Until trials at Naval Postgraduate School (NPS), there had not been an investigation into a setup that could both generate power and explore optimization properties of BMFCs simultaneously. Geometric dimensions are thought to play a large role here. While the exact optimal distance between bacteria and electrode is unknown, it is thought that macrosystems

provide too large an average distance for electron capture to be efficient. Microfluidics provides a first design concept in this research to shrink the bacteria-electrode distance and optimize power harnessing.

A smaller distance between the bacteria and electrodes provides a linearly scaled reduction in voltage losses due to ohmic resistance [10]. The ohmic resistance voltage can be calculated via the following equation:

$$\Delta V = \frac{\delta_w I}{\sigma}$$

where δ_w is the distance between the reference electrode and membrane, I is current density, and σ is the conductivity of the bacterial slurry [10]. Spherical bacterial cells usually have a diameter of less than 2 microns. Cylindrical cells are generally ~1 micron in diameter and up to 10 microns in length [28]. The concentration of bacteria in the fuel cell along with the biomass available to them as a food source greatly determines the amount of charge produced by the bacteria. The amount of charge determines how much energy can be harnessed for powering an external circuit. Thus, the volume to house the bacterial slurry and the distance between the far points of that volume and the nearest electrode are inversely related.

1.3.1 Research Trials at Naval Postgraduate School

In 2019, research trials at NPS yielded average power density outputs of ~120 mW/m^2, with a peak power density of ~160 mW/m^2 after 30 days [28]. These results were nearly four times larger than power density outputs of previous benthic microfluidic designs [28]. The design was a microfluidic, polydimethylsiloxane (PDMS) chip 100 microns wide with a 90 micron ceiling height. PDMS is an organically inert silicon-based substance widely used in biotechnology applications and thought to be bacteria-friendly. The dimensions of the chip were chosen to shrink bacteria-electrode distancing but remain voluminous enough to fit the sediment slurry containing bacteria [28].

The MFC chip used in the 2019 trials and shown in Figure 1.4 had two components: a micro-electrode wiring matrix of a two-dimensional (2D) H-fractal architecture with a chrome on glass base and a PDMS dome template on top of the base. The wiring matrix was fabricated via photolithography and wet-etching methods [28].

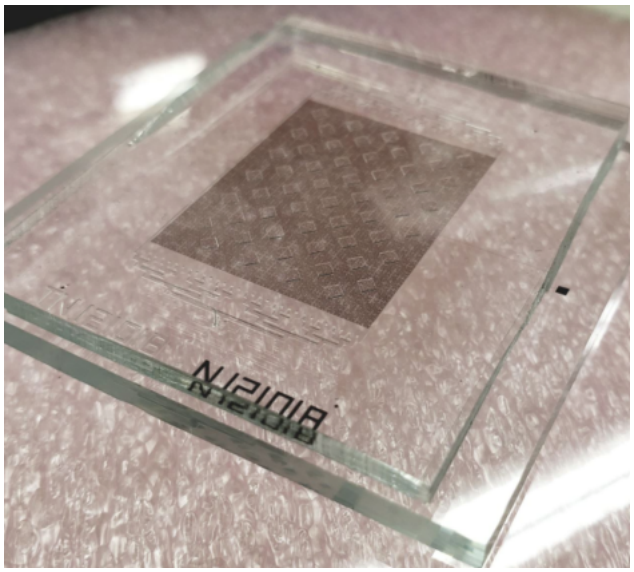

Figure 1.4. Assembled microfluidic MFC chip. Source: [28]

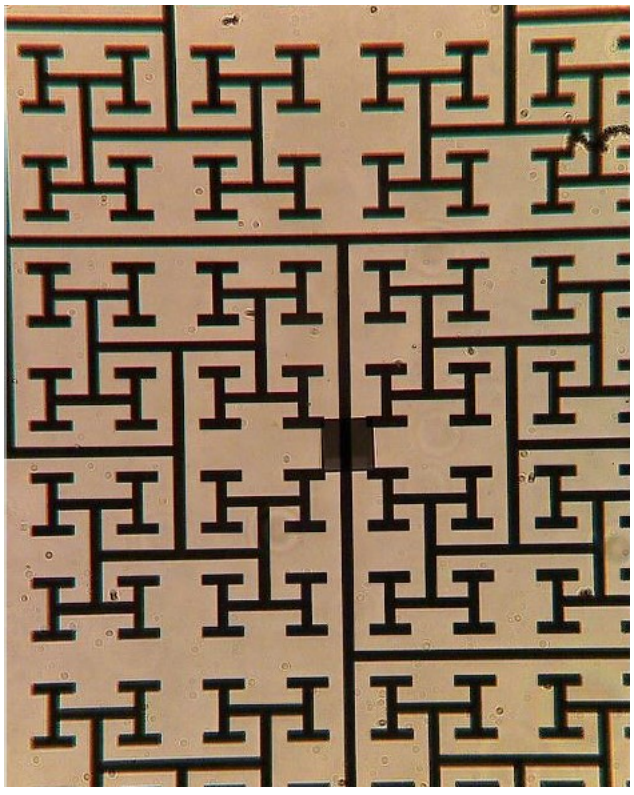

Figure 1.5. A depiction of the chromium on quartz H-architecture of the MFC electrode matrix. Source: [28]

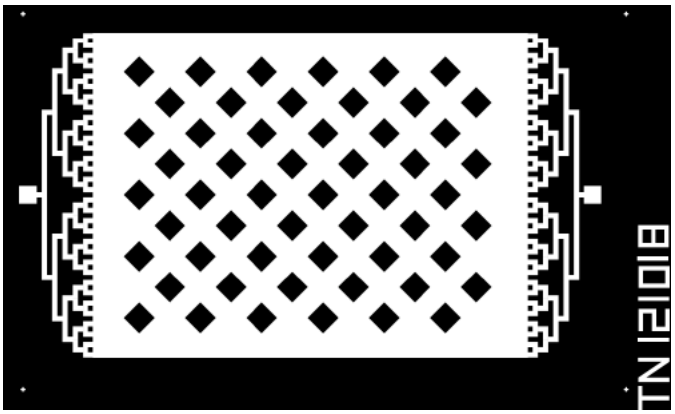

Figure 1.6. A top depiction of the microfluidic dome template that housed bacteria and media. Source [28]

In addition to yielding higher power density outputs, the 2019 research concluded that microfluidic channel architecture, cellular concentration, biomass content, and microelectrode configuration were factors that warrant additional research in improving output power density further [28]. The fabrication of the PDMS dome was also considered time consuming and expensive, especially if it were to scale. Three-dimensional (3D) printing was then considered for producing microfluidic MFC chips.

Scaling 2D architecture chips to 3D is challenging due to the limitations of 3D printing. Currently, there is no existing process to simultaneously print a structural resin with conductive metal for wiring due to the difference in melting points of the materials. This problem creates the need for novel methods of manufacturing. The primary proposed method involves printing the structural resin with sacrificial wax as a filler in the channels, then clearing the wax to bore an empty space to house wiring, bacteria, and media. This clearing process was first demonstrated at NPS in 2022 [29]. The channels were experimentally cleared of sacrificial wax by a combination of solvent, gravity, heat, and pressurized air. The remaining empty channel was then filled with a conductive material to serve as wiring in the chip. The alternative method required embedding conductive material in the resin and directly printing chips from this mixture. It is the population of conductive material in a cleared channel that is the topic of this thesis.

1.4 Carbon Nanofibers

Carbon nanofibers (CNF) have many desirable properties that make them conducive to using them in microfluidic wiring. They have high thermal and electrical conductivities and are low density and lightweight [30]. They can transfer these properties to various thermoplastics, elastomers, ceramics, metals, etc. Due to their high conductivity properties, less concentration loading of CNFs is required when preparing these hybrid materials compared to traditional conductive fillers [31]. The conductivity for pure carbon nanotubes (CNT) can reach on the order of 10^7 Siemens/meter and pure graphene at 10^8 S/m. This is comparable to traditional wiring materials of silver and copper, which have conductivity values on the order of 10^7 S/m [31]. Because of the desirable properties CNFs exhibit, their use in the electrode wiring within a microbial fuel cell device is of keen interest and explored in this research.

CHAPTER 2:
Experimental Methodology

This chapter includes a summary of design concepts of the chips fabricated in 2022 for clearing experiments. The design for those chips was used in populating the channels with conductive material for the continuing research in this thesis. Methods and materials for channel architecture, chip fabrication, clearing methods and results, and wiring injection will also be discussed.

2.1 Channel Design Concepts in 2022

The 2022 research [29] yielded two different designs of channel architecture for 3D printed chips. The first design was a T-channel architecture shown in Figure 2.1. The idea behind the T-channel concept was to capitalize on the fact that microfluidic devices operate in low number (Re) regimes. This quantity is the ratio between inertial forces and viscous forces and has the following relationship:

$$Re = \frac{\rho V L}{\mu}$$

where ρ is fluid density, V is fluid velocity, L is the characteristic length, and μ is dynamic viscosity. When the Reynold's number is low, viscous forces dominate over inertial forces which gives rise to laminar flow. Laminar flow conditions are friendly to confined bacteria and support fluid layer separation between injected conductive wiring and bacterial slurry. The T-channel architecture also supported the concept of self-assembled wiring.

The design of the T-channel features a "T" shaped cross-section (Figure 2.1 A & B). This "T" cross section is printed full of sacrificial wax and entirely cleared to yield a void. Next, a conductive fluid is injected into the "T" void to create the electrode channel. The result from this is illustrated in Figure 2.1 (B) where the yellow represents conductive fluid. The bacterial slurry is then injected into the void in the same manner as the electrode fluid. This method relies on surface tension properties to separate the bacterial fluid and the electrode fluid. A hydrophobic, conductive fluid populated first wets the electrode channel (the bottom yellow strip in Figure 2.1 (C & D)) more easily than an aqueous fluid i.e. the

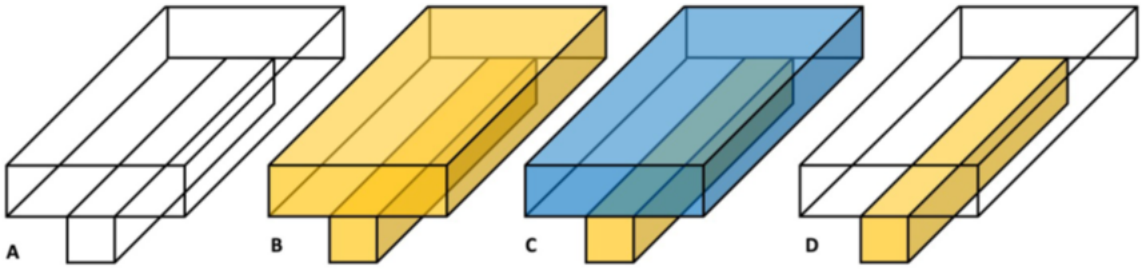

Figure 2.1. Concept depiction of the T-channel architecture. The region in (A) represents a solid space filled with wax. The region in (B) represents the area to be cleared. The blue region in (C) would house bacteria in seawater while the yellow region in (C) would be populated with conductive material to act as the electron transport medium. The (D) region shows the final configuration with wiring in the yellow space. Source: [29]

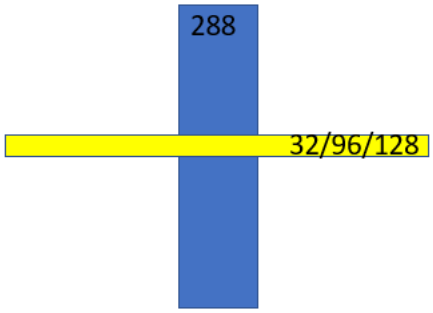

Figure 2.2. T-channel dimensions. The main width was 288 microns, with varying cross-section widths of 32, 96, and 128 microns.

bacterial slurry. Because the slurry is injected last and the flow remains laminar, it flows more easily into the larger portion of the channel (the blue highlighted region in Figure 2.1 (C)) and does not displace the conductive material in the smaller portion of the channel. The result is shown in Figure 2.1 (C). Bacteria are housed in the upper blue region and the wiring fluid is separated and fixed in place in the lower yellow region.

The T-channel dimensions used in this research had a main channel width of 288 microns, with varying cross-void widths. This is illustrated in Figure 2.2.

The second channel architecture design was a simple square channel. This channel was originally designed specifically for the clearing experiments conducted in [29]. Square channels of varying widths were printed with sacrificial material and cleared to create a square void. The purpose of the 2022 experiments [29] was to determine the optimum channel size to facilitate maximum clearing of the void. The smallest channels ~60-100 microns wide were not successful in being cleared. Channels ranging from ~200-900 microns were capable of being cleared to approximately 75% or more. This information was then used to determine the size of the T-channels.

The chips that were produced for the 2022 research [29] (and this work, with minor adjustments) had the following dimensions: 9cm long, 7cm wide, and 2.2mm tall with a 3.1mm tall rim. The chips have a 650-micron diameter port for channel access; this size was intended to accommodate a 1cc, luer tipped syringe.

The 2022 chips were reproduced for this research with subtle changes in material. Two separate batches of chips were fabricated. One batch was made entirely of hard resin (VeroClear-RGD810) including the channels which were filled with sacrificial material SUP706. A second batch used the hard resin as structural support but contained channels made from soft resin (Agilus30 Clear FLX985). Both hard and soft channels were of the same geometry and dimensions. The reasoning behind utilizing two different types of channels of the same geometry was to investigate if CNF accumulation would improve with either configuration.

2.1.1 3D Printer Specifications

The 3D printer used for manufacturing the chips was a Stratasys Objet500 Connex. This model has the capability to print multiple materials in a single run. It uses PolyJet 3-D printing in which resins sensitive to ultraviolet (UV) light are stacked in layers then cured through exposure to UV lamps inside the printer. The primary structural material for the chips was VeroClear-RGD810. The sacrificial material used was SUP706. The VeroClear material is rigid after being cured by UV and nearly transparent. The sacrificial wax material is translucent and is soluble in sodium hydroxide (NaOH) .

A limitation of this printer is the lack of conductive resin commercially available for printing. While the printer can print multiple materials at once, the materials must be

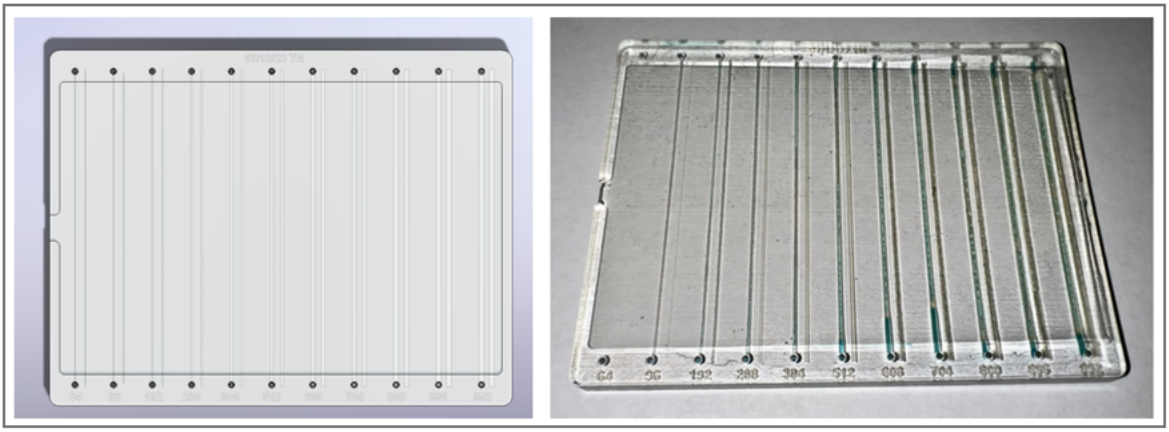

Figure 2.3. An example of a printed chip. To the left is a SolidWorks rendition and to the right is the finished product prior to any clearing treatment. Source: [29]

similar in melting point and structure to accomplish this. For instance, the printer cannot deposit a resin layer on a metal layer, eliminating the possibility of directly printing wiring in the channel. Custom-made conductive resins are possible, however. These are used in PolyJet printing and have small conductive media (nanoparticles) diffused through the resin [29]. On par with the dual resin-metal combination, these custom conductive resins are printable but not in a hybrid mode. They must be printed separately and at low resolutions.

2.2 Chip Processing Procedures and Methods

Both square and T-channel chips were produced for this research, using the same designs from 2022 discussed in Section 2.1. Once the chips were printed, they were cleaned and put through a clearing process to create the channel voids. The clearing process produced expanded channel dimensions which was unexpected and required additional experimentation to investigate the mechanism of expansion. Additionally, the channels were populated with conductive material to serve as the electron transfer medium through a variety of methods. A sample of a chip freshly printed is shown in Figures 2.3 and 2.4.

2.2.1 Channel Clearing

Once printed, the chips were cleared with the procedure outlined in Table 2.1.

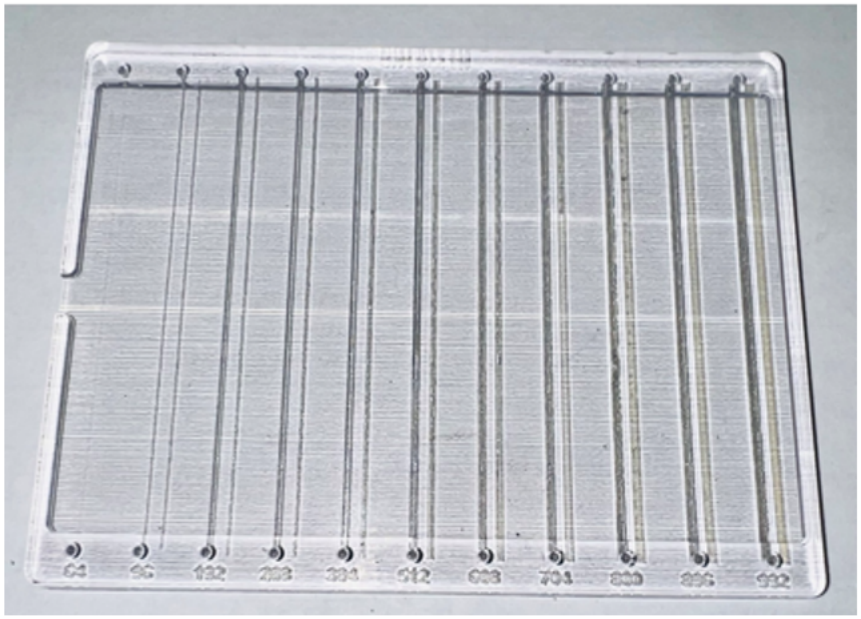

Figure 2.4. Frontal view of a printed chip. Source: [29]

Table 2.1. Procedure for clearing sacrificial wax from printed channels.

1	Remove exterior sacrificial material by hand.
2	Sonicate the chip in 10% NaOH solution for one hour.
3	Rinse the chip with freshwater.
4	Bake the chip in an oven at 80 C for four hours.
5	Remove the chip from the oven and allow to cool to room temperature.
6	With a luer tip syringe, inject the channel with 10% NaOH. Soak overnight if needed.
7	Inject the channel with freshwater to flush NaOH.
8	Inject the channel with isopropyl alcohol in preparation for wiring injection.

The 2022 research revealed that channel widths after clearing were larger than designed. The largest of these discrepancies was a measured channel width of ~200 microns and a design width of 96 microns [29]. This size discrepancy becomes much less pronounced as the design channel width grows larger. This research did not measure design vs. actual width. Instead, the mechanism of this discrepancy was investigated and the knowledge that the chips may be larger than designed was accepted when working with the channels.

There were two hypotheses relating to the expansion of the channels. The first was the

possibility that the printer was off in its calibration or malfunctioning. The second was the possibility that heating the chip in the clearance process was causing the channels to expand. To investigate the latter, melting experiments of the sacrificial wax material SUP706 were performed at two different temperatures. The oven was preheated to 45^oC and 80^oC respectively. For each run, 20 Eppendorf tubes were labeled, filled with approximately 0.5 grams (+/- 0.2) of SUP706 wax material, and weighed prior to heating. The tubes were fixed upright in a perforated holder with lids open and placed in the preheated oven for two hours at respective temperatures. The tubes were removed from the oven after two hours and allowed to come to room temperature. The tubes were then sealed by closing their lids and weighed to determine final mass. Melting i.e. the transition from solid to a liquid, was not observed during heating. The mass loss recorded and observed appeared to be through an outgassing process. The reason for the widening of the channels was attributed to this outgassing process.

2.2.2 Channel Wiring

There were many options explored when determining the best, most practical method of installing electrode wiring inside the cleared channels. The characteristics required of the electron transfer medium included bio-compatibility, minimized distance between bacteria and wiring, the ability to allow water to flow after the wiring is populated (no clogged channels, leave room for bacterial solution), and low resistance or high conductivity. Custom-made resins were considered an option and experiments were conducted to determine if their electrical properties made this viable. The custom resins would not be 3D printed. Instead, the chips would be printed as squares and "T's" and cleared in the usual way, then injected with the custom resin.

Custom resins consisted of mixing various biocompatible, conductive materials such as carbon nanotubes, carbon nanofibers, and graphene with curable resins sensitive to UV radiation. These resins were chosen because they were compatible with the 3D printer. To prepare the custom resin mixtures, the added conductive material was weighed as a target percentage of total mass. Preparations of 1% CNF up to 12% CNF in resin were made. Resin, such as TangoPlus, was weighed and combined with the conductive material. The centrifuge used to thoroughly combine the mixture required at least 30 grams to operate properly, so all CNF mass percentages were based on having at least 30 grams of resin

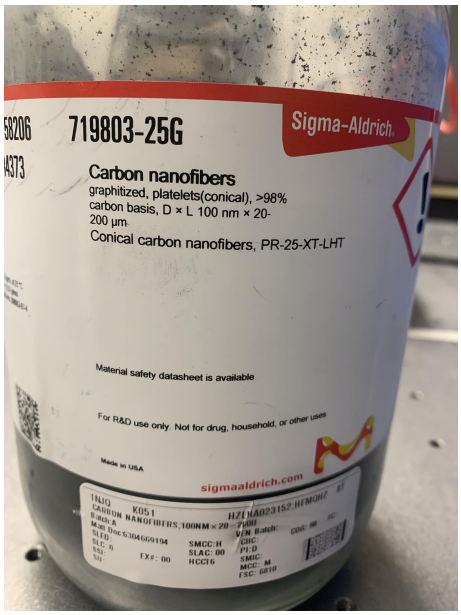

Figure 2.5. A picture of the carbon nanofiber container housing those used when preparing the CNF in isopropyl alcohol solution and the custom resins.

available. The mixing container was then placed in a jig compatible with the centrifuge and the material combined at 2000 RPM for four minutes. The resin mixture was removed from the centrifuge and with a small tool, samples were smeared across the surface of a printed circuit board (PCB) . The circuit board was placed in a UV oven and allowed to cure for eight hours. Resistances were then measured across the PCB and recorded for each material.

The PCB experiments acted as a baseline for wiring the voided channels. While higher concentrations of CNF in resin yielded better conductive results, they were not practical in a microfluidics application due to high viscosity. The top performer was 12% CNF in resin for conductivity but had the consistency of the children's toy Play-Doh. It was not possible to draw this mixture into a luer-tipped syringe and subsequently inject it into a small ~200-900 micron channel. The only mixture capable of being drawn into a syringe and injected was 1% CNF in resin. A concentration of 1% CNF in resin was not a top conductivity performer in the PCB experiments. Nevertheless, a channel trial was conducted with it. The same preparation process previously discussed in this section was performed and the 1% CNF in resin was injected into a T-channel chip. Managing to inject a full syringe volume through

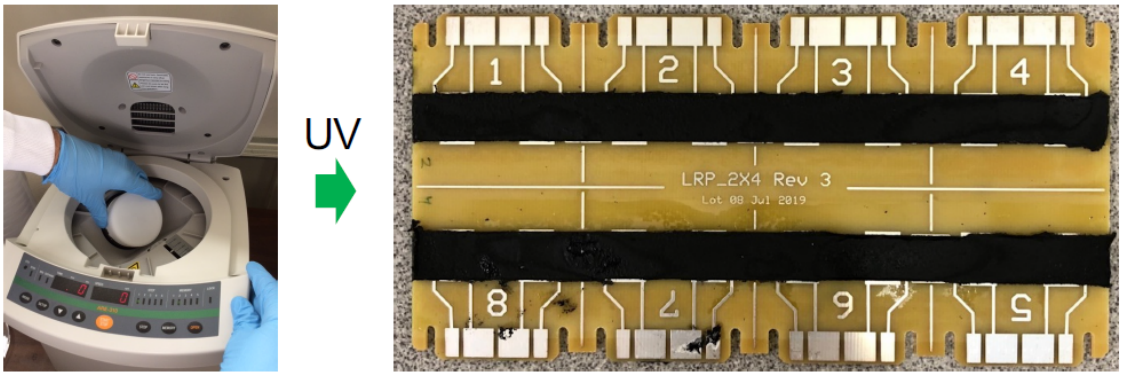

Figure 2.6. Photographic demonstration of custom resin PCB preparation. The solution is mixed in a centrifuge (left), smeared on the PCB, then cured in a UV oven.

the channel proved difficult; the luer tip of the syringe continually became clogged when feeding the material. Once the channels were injected with the 1% CNF in resin, the chip was placed in the UV oven to cure the resin in place. This also yielded problems. The addition of black CNF material to translucent resin appeared to cause the resin to be much less sensitive to UV light. This required a substantially longer curing time, up to 16 or more hours. The CNF in resin mixture revealed itself to still be wet when attempting to take resistance measurements after lesser curing duration. Once cured, steel stub tube pins were inserted into the entry and exit ports of each channel to measure the internal resistance. These resistances measured for 1% CNF in resin populated in the T-channel chips were not promising and exceeded the limit of the meter in all cases.

When the custom resins proved to be impractical in a microfluidics application due to viscosity, an alternate delivery method of CNFs to the channel was investigated. Suspending CNFs in a less viscous liquid was the preferred mechanism due to the need for injection in the micro-channels. CNFs were mixed by volume into water, soapy water, and isopropyl alcohol. Each mixture was easily drawn through a syringe, but the luer tip needle continually clogged with clumps of CNFs when attempting to inject under pressure in all three cases. Sonicating the CNF mixtures in a water bath solved this problem. Isopropyl alcohol was then chosen as the delivery liquid due to its evaporative properties. The desired goal was a fixed-in-place CNF wiring network; the liquid was to be used for delivery of CNFs only. So

Table 2.2. CNF in isopropyl alcohol channel wiring procedure.

1	Prepare 3mg/10mL CNF in isopropyl alcohol solution.
2	Sonicate CNF in isopropyl alcohol solution for 15 (5 after first injection) minutes.
3	Inject CNF solution into cleared channel. Flush full syringe volume.
4	Bake the chip (oriented flat) at 80^oC for 3-4 hours.
5	Let cool to room temperature. Measure the resistance across the channels.
6	Repeat steps 3-5 until resistance no longer lowers after final injection (5-6 iterations).

the ability to quickly rid the channels of delivery liquid through evaporation was a positive.

The CNF delivery mixture utilized consisted of 3 mg CNF in 10 mL of isopropyl alcohol. CNFs were weighed in a container and isopropyl alcohol added directly to this container by volume. Chips were injected following the procedure outlined in Table 2.2. A dry-cycling process was used by baking the chips. Evaporating the isopropyl alcohol and drying the channels fixed the CNFs in place. Additional injections and dry-cycles formed a CNF matrix inside the channels by accumulation.

When the channels reached a steady resistance after final CNF injection, they were injected with freshwater. This was to ensure they could convey additional delivery liquid to add the benthic bacteria in the future. A positive flow of water also demonstrated the ability to house the bacteria above the CNF wiring matrix created by dry-cycling.

Images of the channels were taken under a microscope after each injection and dry-cycle of CNFs. Six images were taken along every channel length for each iteration to represent the average CNF concentration. Injection #3 of the T-channel chips did not have images due to a lab error.

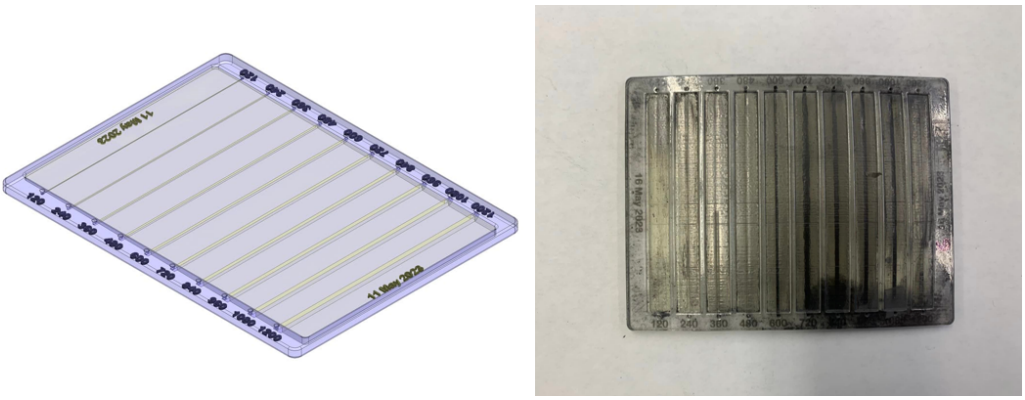

Figure 2.7. Soft square channel example. Pictured to the left is a SolidWorks rendition of the square soft channels used in this research. Pictured to the right is a soft square chip after it has been cleared and dry-cycled with CNF injections. Channels 600 microns and larger are populated with CNFs as seen by the darkening of those channels. Their sizes are indicated by the numbers at the top and bottom, which are also the locations of the entry and exit ports.

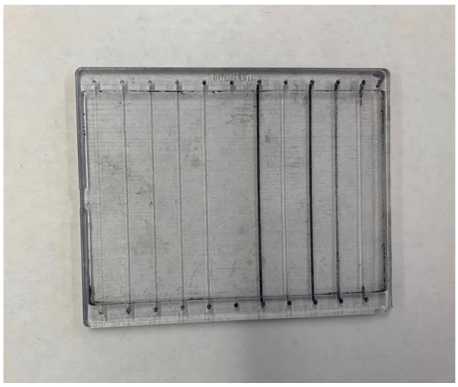

Figure 2.8. Pictured is a square hard channel chip after being cleared and dry-cycled with CNF injections. Darkened channels are fully populated with a CNF wiring matrix. Channels to the left of the chip were less than 500 microns and were too small to clear or did not accept CNFs readily. The channel second to the right is an example of a channel that only accepted two injections, compared to the one to its left which accepted a full five.

CHAPTER 3:
Results

This chapter displays the results of the clearing process mechanism and those obtained in conductivity testing completed in custom resin and isopropyl alcohol. Section 3.1 presents the results of mass loss outgassing in clearance. Section 3.2 presents the findings of custom resin resistances on printed circuit boards. And Sections 3.3 and 3.4 show the results of T-channel resistances and square channel resistances respectively, after being dry cycled with CNF in isopropyl alcohol solution.

3.1 Mass Loss Outgassing

Melting experiments showed the mechanism of sacrificial wax removal to be due to outgassing. Channel widening was also attributed to this process and consistent with roughly 10% widening. The experiments conducted at 80^oC yielded an average mass loss of 6.92% with a standard deviation of 2.41%. Experiments conducted at 40 C did not demonstrate mass loss and were not statistically significant.

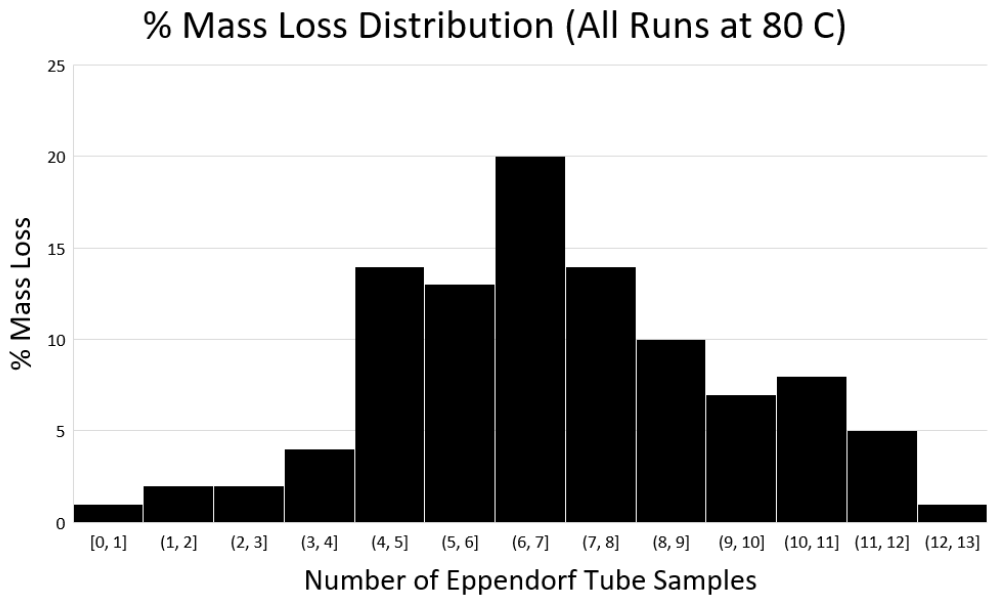

Figure 3.1. Histogram displaying mass outgassing results. Average mass loss was 6.92% with a standard deviation of 2.41%.

3.2 Custom Resin Resistances

The custom resin mixtures created with CNFs, CNTs, carbon mesoporous, and graphene in resin at varying weights yielded promising conductivity results. The best results were with CNF at 12% weight in TangoPlus resin. While this mixture was possible to smear and cure on a PCB, it was much too viscous to be considered as an injection in microchannel geometries. The CNFs in TangoPlus resin were injectable only at 1% weight. CNFs at 1% weight demonstrated resistances not detectable by the probe which had a maximum overload resistance of 220 MΩ. Additionally, when injected in the microchannels, the custom resins required several eight hour UV cycles to cure (over 24 hours) compared to on the PCB which required only one cycle.

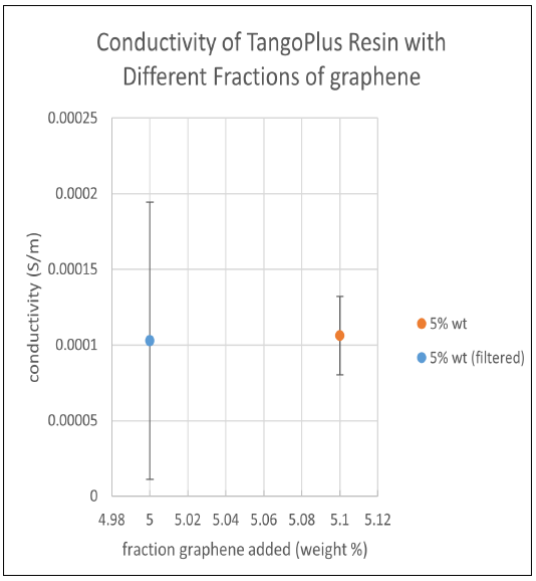

Figure 3.2. Graph depicting conductivity results of graphene custom resins at varying weight fractions.

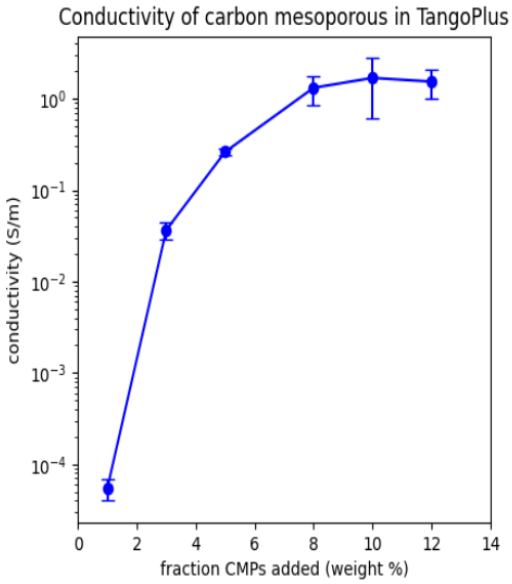

Figure 3.3. Graph depicting conductivities of carbon mesoporous custom resins at varying weight fractions.

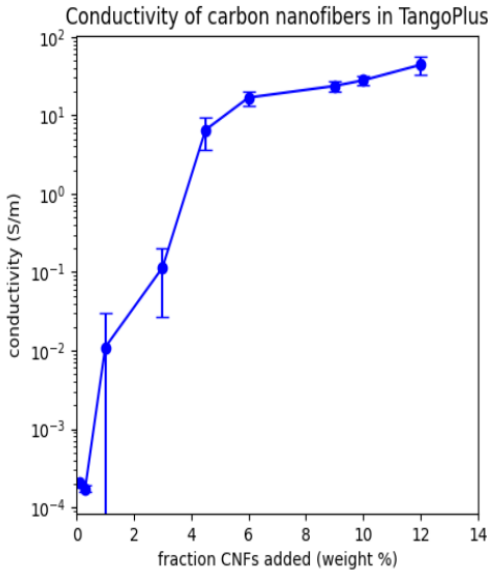

Figure 3.4. Graph depicting conductivities of carbon nanofiber custom resins at varying weight fractions.

3.3 T-Channel Resistances After Dry-Cycling with CNF in Isopropyl Alcohol

T-channel resistances performed worse than the square channel batches. They accepted the same number of CNF injections (approximately five) as the square channels, but final resistances were consistently around 50 kΩ compared to values as low as 6 kΩ in the square channels. T-channels also had a more difficult time conveying water after final injection of CNFs. That is, the ability to populate benthic bacteria after the final dry cycle was not demonstrated consistently after five injections. This indicated a need to scale back by at least one CNF injection to show a conveyance of water. Images were taken under a microscope to document the accumulation of CNF. The chips darkened after each subsequent injection, demonstrating higher CNF concentration with every iteration. An example of these images is shown in Figure 3.17.

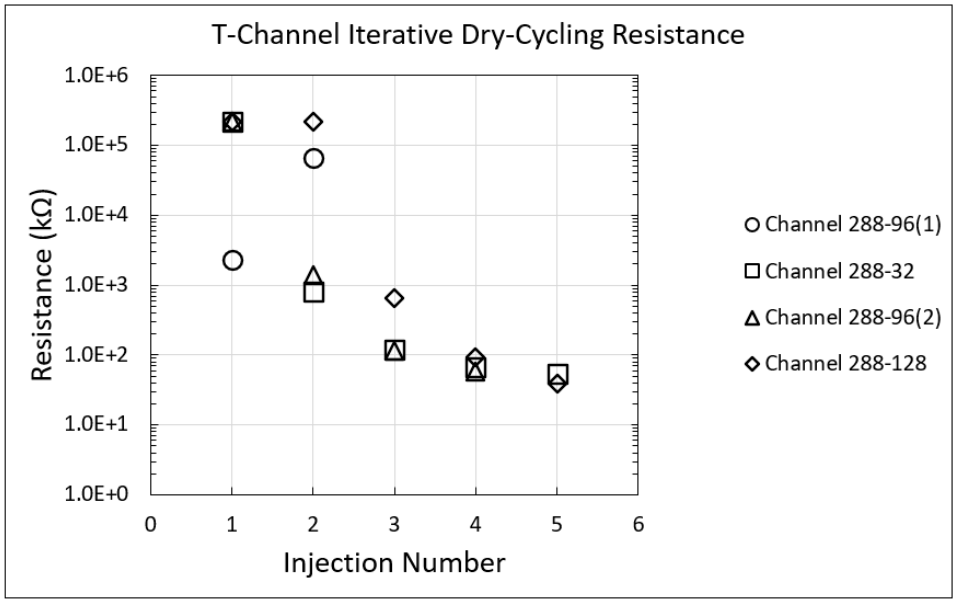

Figure 3.5. Graph depicting resistance results for four channels after dry-cycling T-channels with CNF in isopropyl alcohol. Channel naming convention assigned the first number to represent the main channel width, with the second number representing the varied T-channel cross section width. Error bars are not shown due to being smaller than the point markers.

3.4 Square Channel Resistances After Dry-Cycling with CNF in Isopropyl Alcohol

Square channel resistances showed consistent results across both hard and soft channels of the same geometry and dimensions. Both configurations received the CNF mixture similarly in the number of injections accepted before clogging or leveling out in resistance. Square channels had better results practically and quantitatively than the T-channel geometry. That is, CNFs were easier to inject in the square channels and the number of iterative injections was higher, leading to lower final resistances.

3.4.1 Soft Channel Resistances

The soft channels were created from Agilus30 Clear FLX985. All channels above approximately 600 microns accepted up to about five iterations of injections. Injections were

continued until resistance leveled to a consistent value, or the channel became clogged and would no longer accept more CNFs. Channels below 600 microns are not shown graphically as they did not accept more than two injections before becoming clogged. Each channel shown graphically was able to convey water after its final CNF injection. That is, water was still able to pass through the channel after the CNF wiring had been populated, demonstrating the ability to add benthic bacteria after this dry-cycling process. Final resistances after five injections varied from approximately 10-40 kΩ. All plots that show more than one channel in a single figure have the naming convention assigning the first number to differentiate each chip, with the second number describing the channel width.

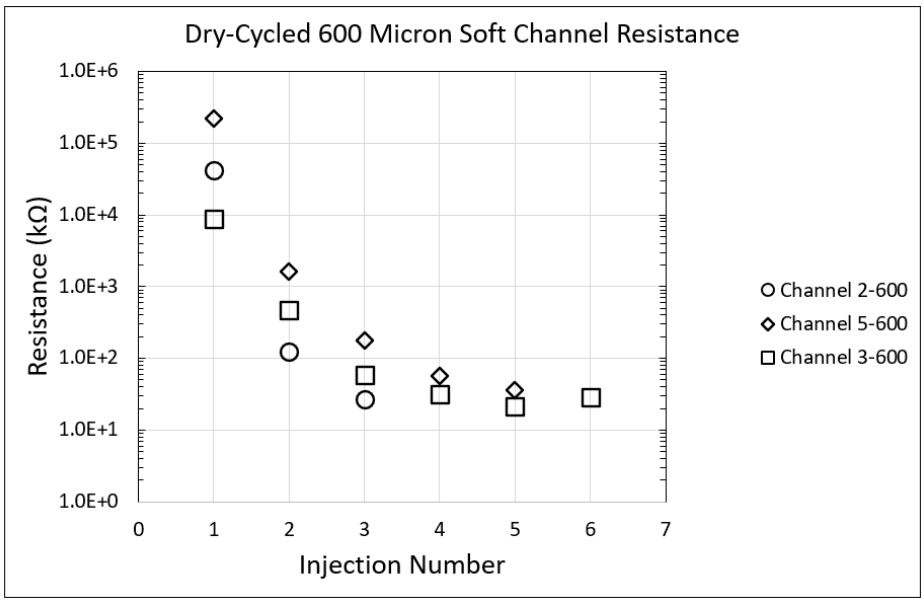

Figure 3.6. Log-scale graphs depicting resistance over injection number for 600 micron square channels. Error bars are not shown due to being smaller than the point markers.

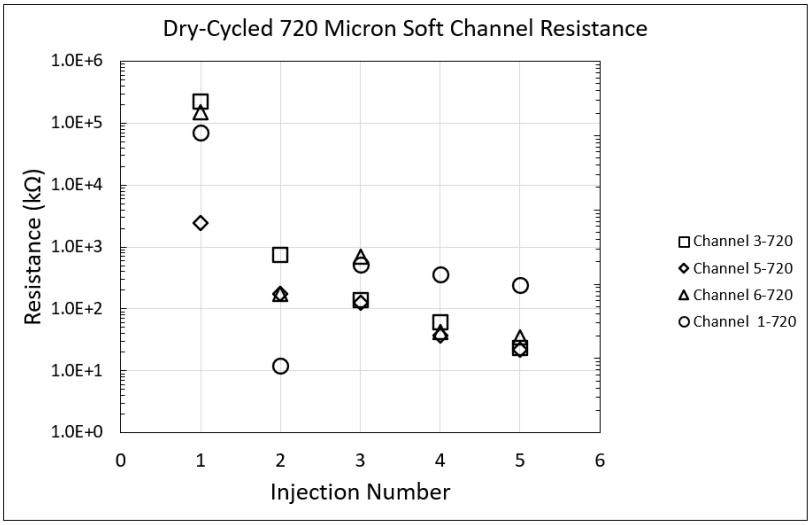

Figure 3.7. Log-scale graphs depicting resistance over injection number for 720 micron square channels. Error bars are not shown due to being smaller than the point markers.

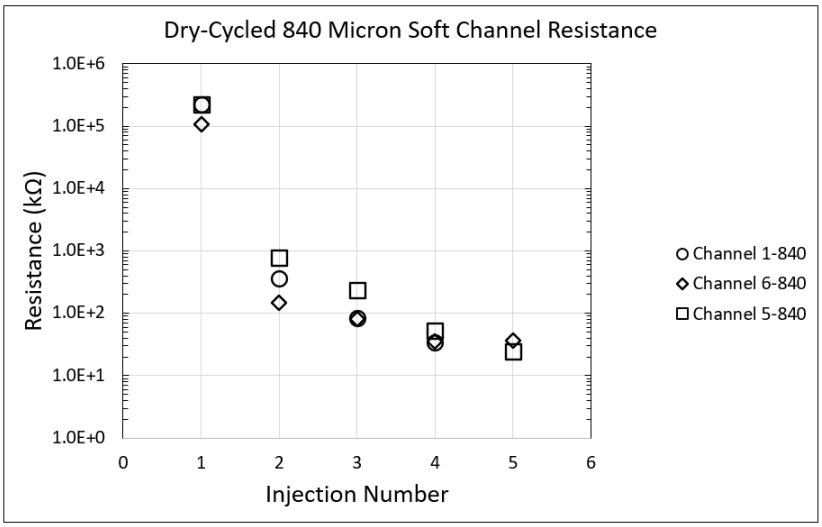

Figure 3.8. Log-scale graphs depicting resistance over injection number for 840 micron soft square channels. Error bars are not shown due to being smaller than the point markers.

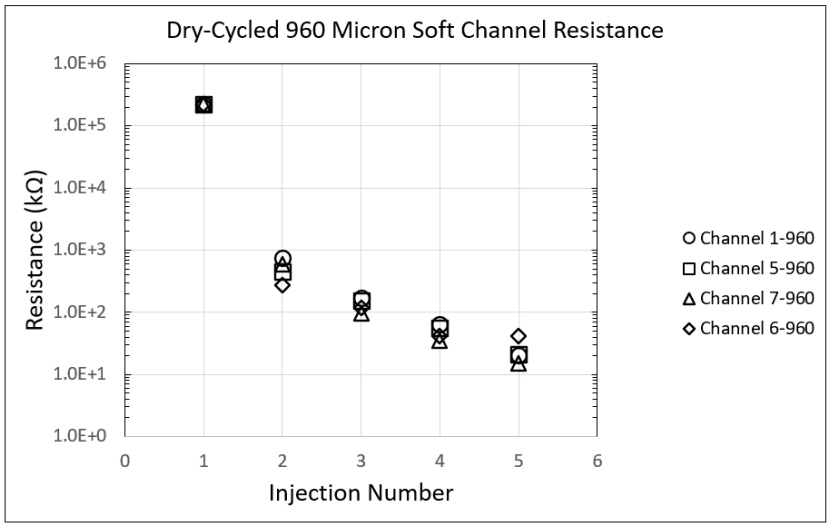

Figure 3.9. Log-scale graphs depicting resistance over injection number for 960 micron soft square channels. Error bars are not shown due to being smaller than the point markers.

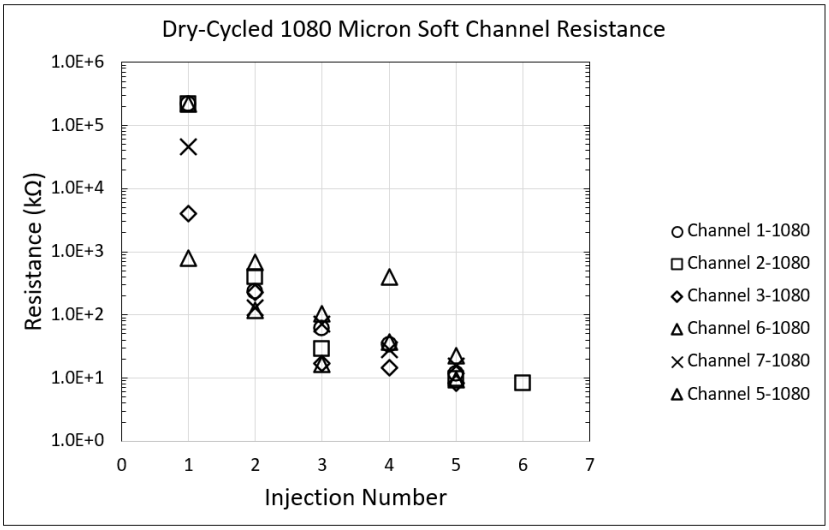

Figure 3.10. Log-scale graphs depicting resistance over injection number for 1080 micron soft square channels. Error bars are not shown due to being smaller than the point markers.

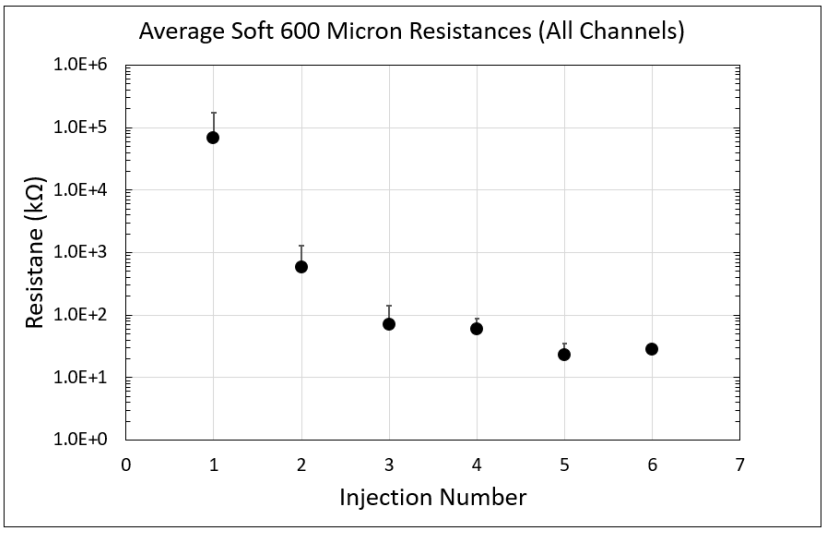

Figure 3.11. Log-scale graph depicting averages over a single channel width in multiple chips. Compiled 600 micron channel chips are shown. Error bars show standard deviation over a single channel width in multiple chips.

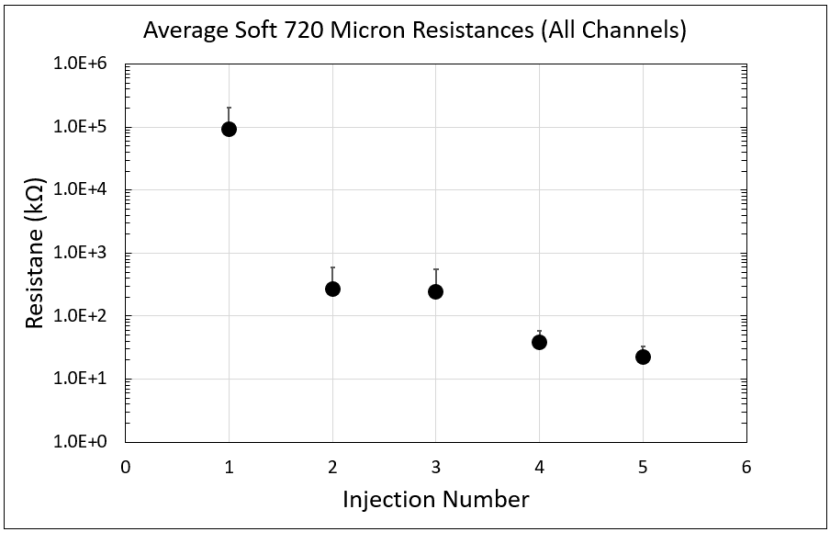

Figure 3.12. Log-scale graph depicting averages over a single channel width in multiple chips. Compiled 720 micron channel chips are shown. Error bars show standard deviation over a single channel width in multiple chips.

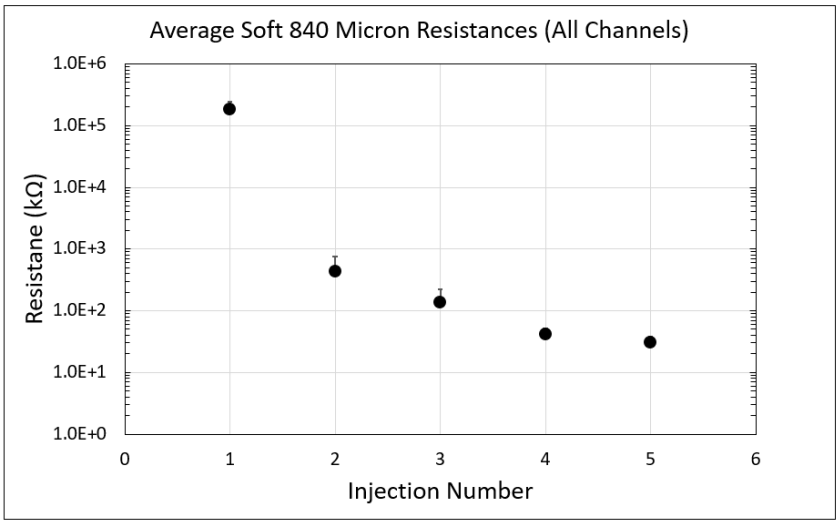

Figure 3.13. Log-scale graph depicting averages over a single channel width in multiple chips. Compiled 840 micron channel chips are shown. Error bars show standard deviation over a single channel width in multiple chips.

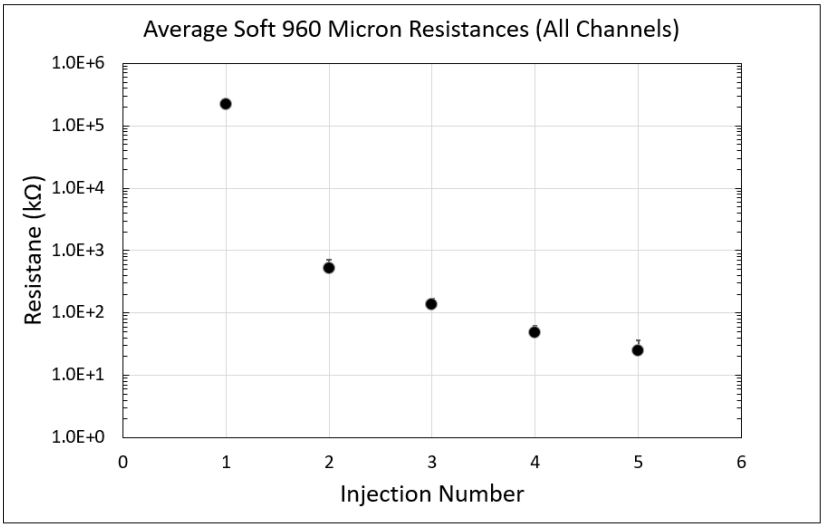

Figure 3.14. Log-scale graph depicting averages over a single channel width in multiple chips. Compiled 960 micron channel chips are shown. Error bars show standard deviation over a single channel width in multiple chips.

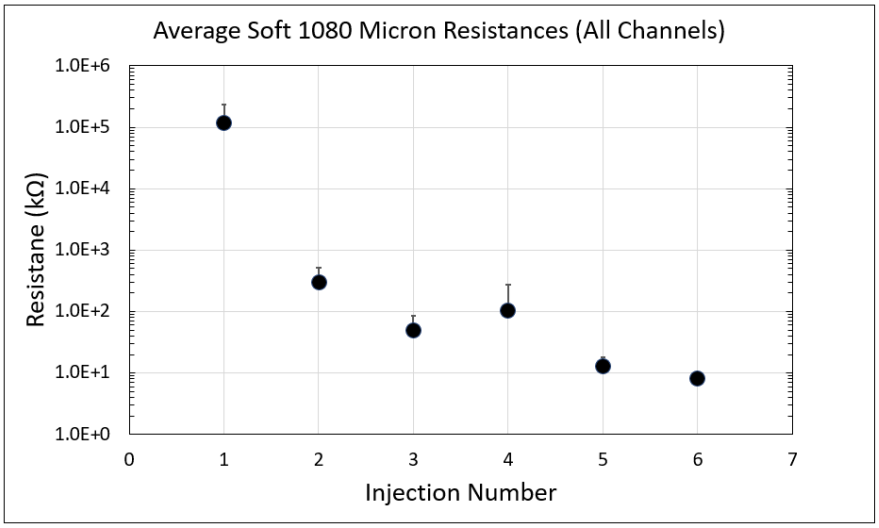

Figure 3.15. Log-scale graph depicting averages over a single channel width in multiple chips. Compiled 1080 micron channel chips are shown. Error bars show standard deviation over a single channel width in multiple chips.

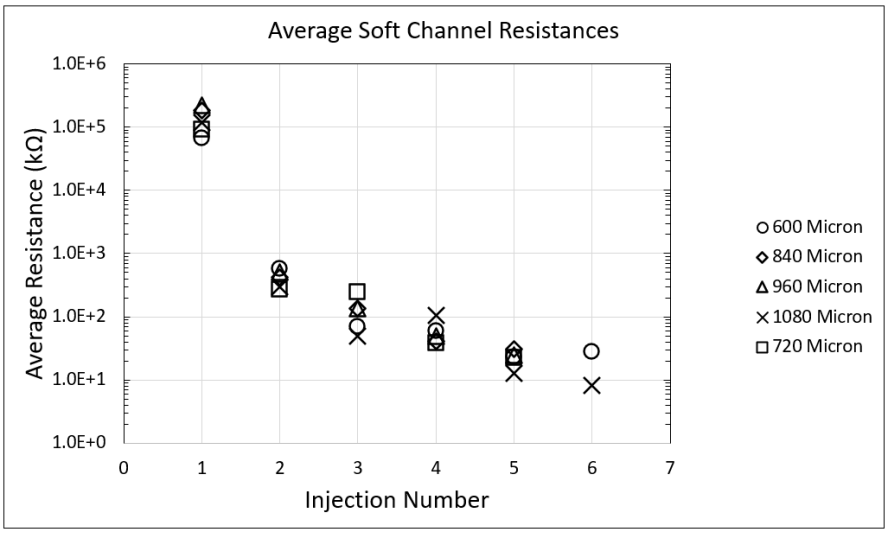

Figure 3.16. Compiled average resistances across all channels in all chips. Error bars are not shown due to being smaller than the point markers.

3.4.2 Hard Channel Resistances

The hard channels were created from VeroClear-RGD810. Hard channels larger than 600 microns accepted up to about five injections which was consistent with soft channel behavior. Channels smaller than 600 microns would become clogged by the third injection. Final resistances ranged from approximately 10-20 kΩ. As discussed in Section 3.3, images were taken under a microscope to observe and verify the rising concentration of CNFs visually. Images were taken for all configurations (T-channel, soft square, and hard square) and darkening was observed for all as well. Only one example is needed to illustrate this phenomenon and is provided in Figure 3.17. All plots that show more than one channel in a single figure have the naming convention assigning the first number to differentiate each chip, with the second number describing the channel width. Figures 3.18-3.22 show an identical trend compared to the soft channel data. The accumulation of CNFs is clearly observed both visually and through a lowering resistance measurement over injection number. This indicates rising conductivities over injection number.

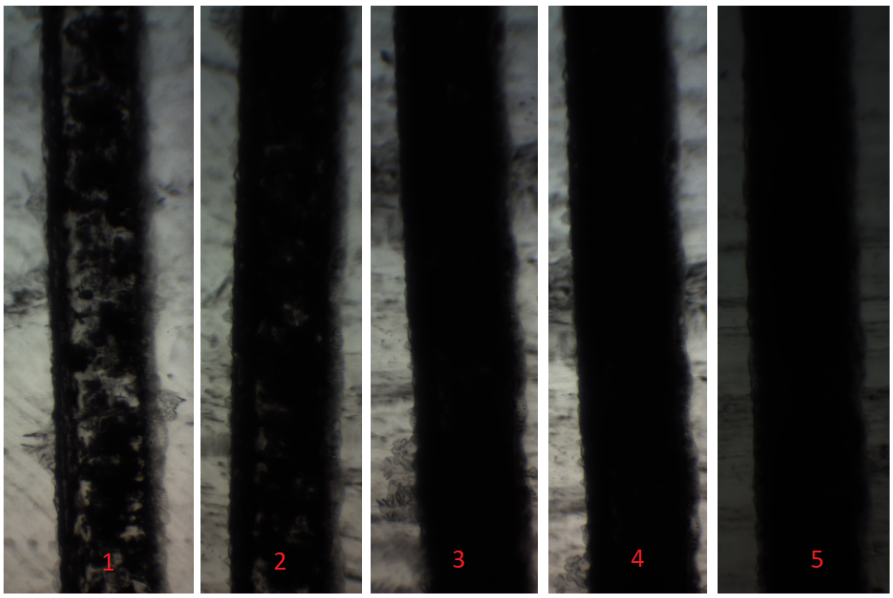

Figure 3.17. Images taken under a microscope of the hard channel 4-764. The channel is 764 microns wide and photographed at 0.4 magnification. Injection iterations go left to right, from the first injection to final fifth injection.

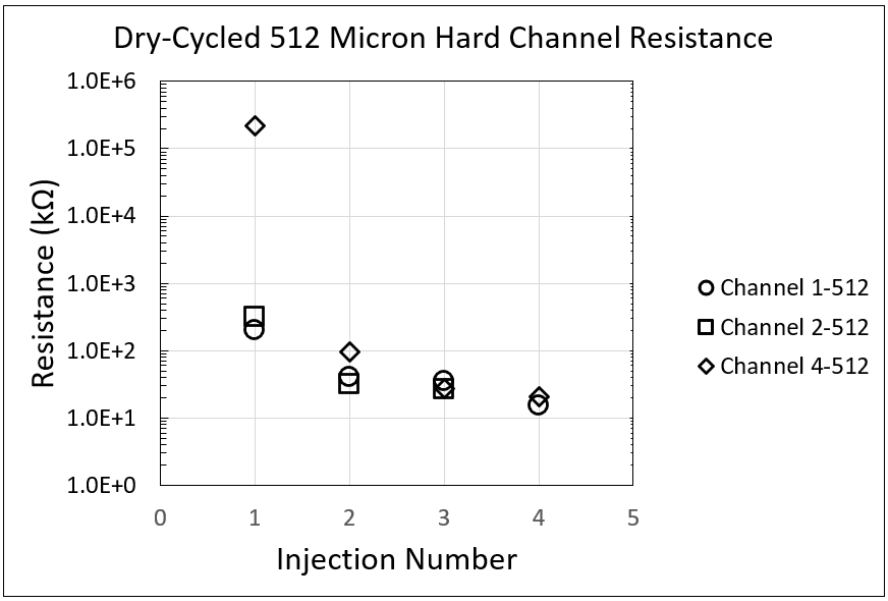

Figure 3.18. Log-scale graph depicting 512 micron hard channel resistances. Error bars are not shown due to being smaller than the point markers.

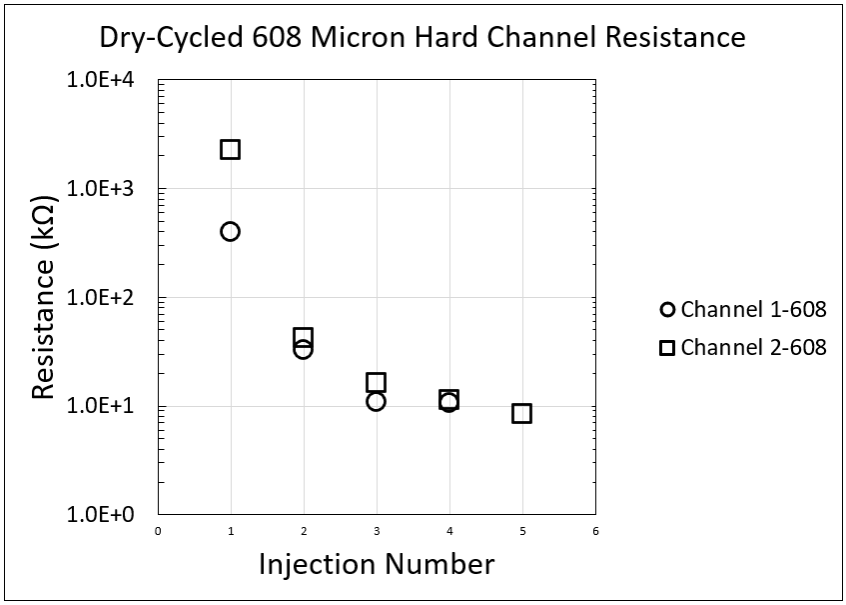

Figure 3.19. Log-scale graph depicting 608 micron hard channel resistances. Error bars are not shown due to being smaller than the point markers.

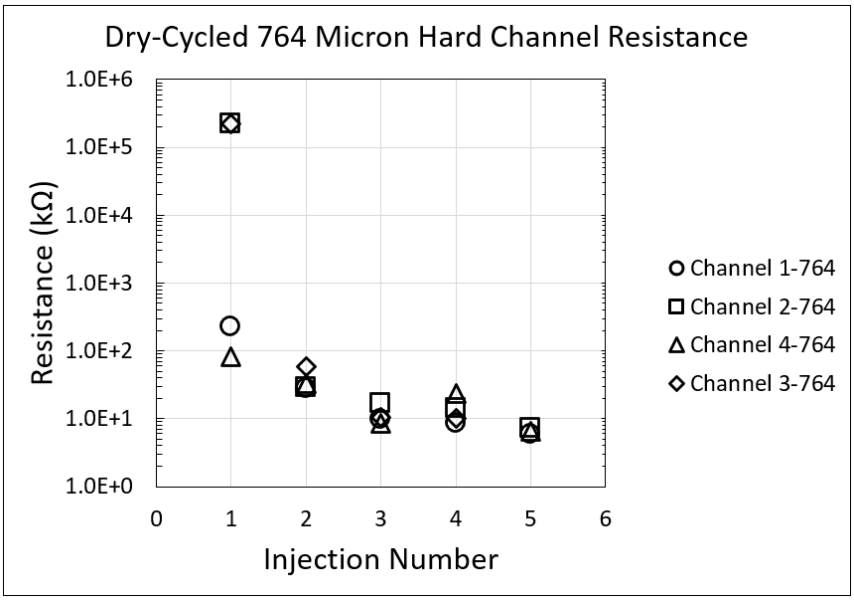

Figure 3.20. Log-scale graph depicting 764 micron hard channel resistances. Error bars are not shown due to being smaller than the point markers.

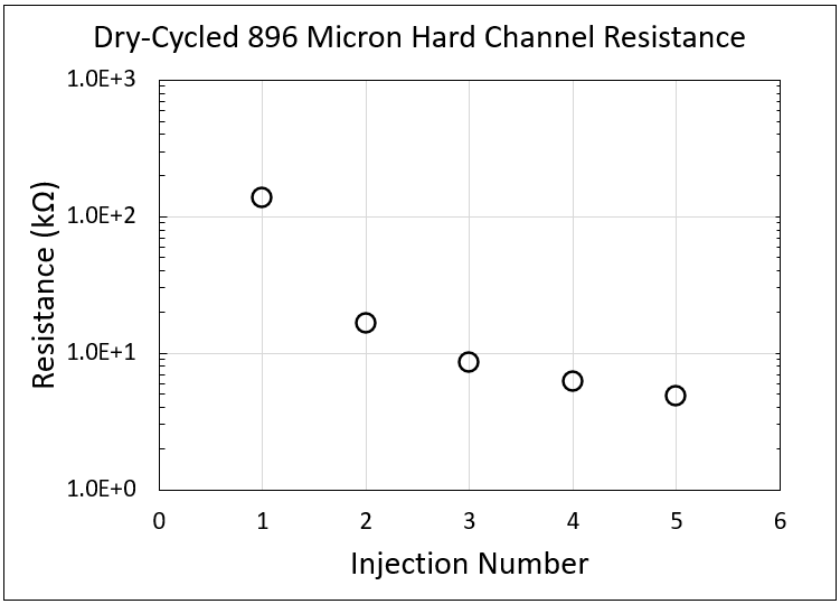

Figure 3.21. Log-scale graph depicting 896 micron hard channel resistances. Error bars are not shown due to being smaller than the point markers.

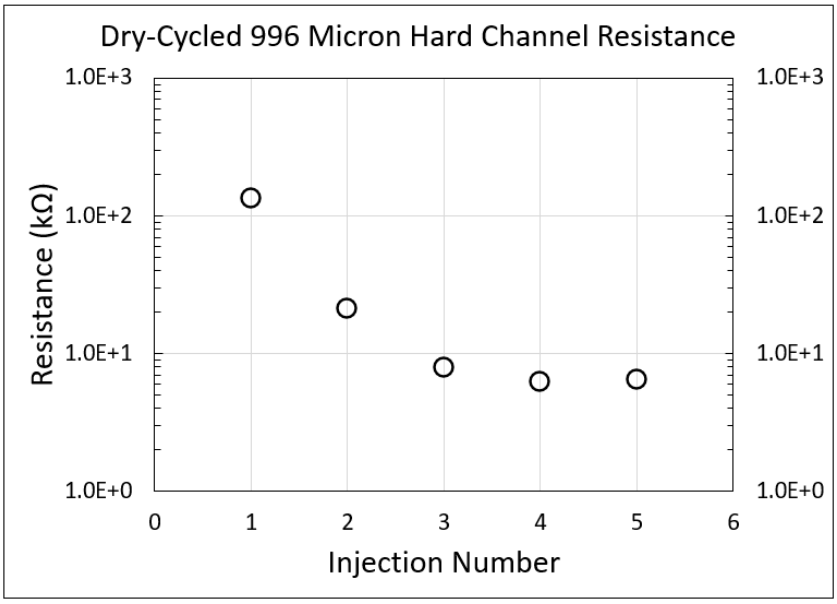

Figure 3.22. Log-scale graph depicting 996 micron hard channel resistances. Error bars are not shown due to being smaller than the point markers.

THIS PAGE INTENTIONALLY LEFT BLANK

CHAPTER 4:
Discussion

This section discusses the results presented in Chapter 3 to include sources of error and uncertainty. Furtherance of this research is also discussed through possible avenues of potential investigation.

4.1 Mass Loss Outgassing, Custom Resins, and T-Channel Resistances

The melting experiments showed the primary mechanism of mass loss to be due to outgassing. This loss was only statistically significant at 80^oC. This explained the widening of the channels, though the exact method the mass exits the chip is still up for debate. In the 2022 trials, chip orientation (vertical or face down) while baking in the oven was thought to be a significant factor in clearance percentage. This does not appear to be the case. Melting of the sacrificial wax does not occur, and so there is no dripping from top to bottom of any liquid that would exit the channel. It is unknown if the outgassing process occurs through the pores of the resin or if the presence of entry and exit ports on the end of each channel are what allow the gas to escape. This is relatively unimportant for the clearance of these open-ended square chips, but could be relevant in future designs that may have different geometries. Different geometries may have different entry and exit locations, or none at all. This would greatly affect the way future geometry chips are cleared and wired.

The custom resins provided valuable resistance information when investigating the optimal concentrations of CNF in resin. However, this path was not taken when it was discovered that the required concentration of CNF in resin needed to have any readable resistance caused the fluid to be too viscous to draw through a syringe, let alone inject into a microchannel. The custom resins may prove useful in other projects where PCBs are the primary delivery vehicle of electrical wiring. Custom resins may also be relevant in hybrid 3D printing, and the data obtained in this research will be helpful in predicting resistances when attempting to directly print CNF embedded resins into a structure. For the purposes of microfluidic channel injection however, the custom resins are a dead end.

The T-channel chips were the first chip design to be processed in this research. The T-channels were the first to be injected with CNF in isopropyl alcohol due to their availability from attempting self-assembled wiring. Recall the T-channel design was originally created to facilitate self-assembled wiring (Section 2.1). This method relied on the surface tension of water and its interaction with a CNF embedded material (a custom resin). Due to the viscosity limitations of the custom resins, self-assembled wiring was abandoned as a simple way to populate wiring in the channels. But with T-channel chips already manufactured, they were injected with CNF in isopropyl alcohol as an experimental carrier fluid. It became apparent that the CNFs were accumulating as the channels darkened. This could be seen by the naked eye and was photographed through a microscope. Resistance measurements quantitatively verified this observation. This accumulation of CNFs drove the revisiting of the square channel design. The T-channel cross sections were smaller than the square design and did not clear as well. Additionally, the T-channels clogged with CNF at saturation and would not express water through the channel after wiring. Because maximum saturation accumulation was required for achieving lowest possible resistances, it was thought that a larger channel could support higher concentrations of CNF. A larger channel at a CNF resistance saturation would also support water passing through after final injection. A simpler square channel would not have the complexities of a cross section and would make it easier for this accumulation to occur. T-channels were not reprinted, and like the custom resins, were abandoned for moving forward as a viable optimized BMFC design.

4.2 Soft Square Channels

The purpose of the soft square channel design was to determine if there was an advantage in channel material for CNF accumulation and subsequent wiring. The results of CNF wiring in the soft square channels showed a final average resistance of approximately 20 kΩ across all channels larger than 600 microns. Channels smaller than 600 microns either did not clear adequately, or did not accept more than two or three CNF injections before becoming clogged. Channels smaller than 600 microns can be eliminated for design dimensions in the future. Each channel larger than 600 microns could receive five or six injections before reaching a resistance that did not change after subsequent injections. This was considered the "saturation" point of CNFs in the channel. This saturation point manifested itself as a final resistance of approximately 10-30 kΩ in most channels. All channels larger than

600 microns were capable of expressing water after reaching this final resistance. This demonstrated that the room required for bacteria to be housed in the channel still existed after wiring. Size did not appear to affect final resistances. First and second injection milestones were quite variable across different channel sizes, however final resistances after a fifth or sixth injection were consistent.

In presenting the resistance results, many plots did not display error bars due to scale. While the resistances shown were in the tens of kΩ, the standard deviation was typically in the tenths or hundredths; this was at least two or more decimal places difference for most data points. And so they were difficult to include without compromising the displayed points. In the average plots, however, they were included. The average plots were created by taking the average resistance across each injection over one size. For example, there were four 720 micron channels. Four resistance values for the first injection were used to calculate the total average resistance after one injection for a 720 micron channel. This was repeated for subsequent injections to generate a plot of average resistances at each injection milestone for one size of channel. The error bars shown on these plots are only the standard deviation of the sample population comprised of the resistance values used to calculate the average at each milestone. They do not display other propagated errors.

A source of error in the average plots is the inclusion of overflow data points recorded during early injections. Many channels yielded an "overflow", or unreadable resistance, due to it being too high after their first injection. CNFs at this stage had not accumulated enough to show substantial resistance measurements when placed under a current. A second injection would nearly always populate enough CNF for a resistance measurement. The overflow measurements were included in the plots of averages as the maximum reading of the resistance meter, which was 220,000 kΩ. The actual resistance of these data points was unknown. These 220,000 kΩ overflow points are also included in the plots of individual channels, but these points are not used to calculate values and so there is no error introduced in that analysis.

Additionally, the method of obtaining both the resistance and standard deviation from the meter involved using a meter function that stored the last 100 readings and calculated values from them. The average and standard deviation from these stored 100 readings was recorded. This is a potential source of error but a significant improvement from the

alternative, which would involve relying on human judgment. Someone would have to look at the meter and observe minimum and maximum values during fluctuations and determine a standard deviation this way. Meter fluctuations were very common. A similar method would have to be used to determine the average.

Meter fluctuations, or rather the source of these fluctuations, are another source of error. Resistance readings would fluctuate more during earlier injection milestones due to the lack of CNF saturation. The CNF wiring matrix had more gaps and discontinuities after one or two injections when compared to after a fifth or sixth injection. As expected, applying a current across a discontinuous path would cause the resistance to "jump" and not hold a consistent value at a single point in time. The general trend of standard deviation was on the order of tens of kΩ starting with the first injection and gradually became tenths and hundredths of kΩ for subsequent injections as the CNF matrix built up. Again, this was not large enough to display on a log plot, but demonstrates achieving higher CNF saturation, and therefore continuity of wiring and current, in the channel as injections progressed.

4.3 Hard Square Channels

The hard square channels behaved similarly to the soft square channels. There was no quantitative evidence that one material was more desirable than the other for achieving maximum CNF saturation, or lowest resistance values. All outcomes were on the same order of magnitude. Hard channels accepted the same number of injections and expressed water similarly after final CNF injection. Final resistances were approximately 10-30 kΩ. Standard deviations followed the same trends and were on the same order of magnitude as those discussed in Section 4.2. Channel sizes larger than 600 microns were also the top performers, identical to the soft channels.

A data point that is currently unknown is whether a hard or soft channel is preferred for a benthic bacteria population housed in the channel. While size and material did not affect final resistance outcomes, these factors could make a difference in power output when bacteria are introduced. Size could affect the bacteria's proximity to the nearest CNF, for instance. And the bacteria could prefer contact with soft over hard resin, or vice versa.

4.4 Future Work

The final product this work is striving toward is a network of self sustaining BMFC stack geometries. Many of these chips stacked together and electrically connected would produce power to sustain various instruments and equipment as discussed in Chapter 1. In other words, BMFC power cubes are the end goal.

The next step after achieving a viable CNF wiring matrix procedure as has been presented in this thesis is to test with live bacteria. It has been theoretically demonstrated that bacteria can still be housed in the channels with the CNF matrix by flushing water after final injection. The bacteria will be added to the channels and allowed to conduct their biological processes over a period of 30-60 days while measuring the power output of the configuration. In collaboration with biologists on this project, they have expressed the desire to house bacteria in a lengthier channel. They believe this will be an improvement for the bacteria to undergo their biological processes and for ease of power measurement in the San Diego laboratory where this will be done. With the square channels in this thesis presented as a proof of concept for dry-cycled CNF matrix wiring, and a baseline for expected resistances, lengthier designs can easily be 3D printed to accommodate this request. The CNF injection procedure can be scaled to varying geometries provided that geometry is an injectable volume.

A current alternative channel design in the works is a spiral geometry. The channels maintain their square cross section. To keep the chip as a whole small, the channel spirals around in a circle to achieve additional length vice being a straight line from entry to exit. The clearance procedure is predicted to be more difficult for this geometry and may require longer baking times or further NaOH treatment. This relates to the unknown outgassing phenomenon discussed in Section 4.1. If the mass outgassing occurs through the pores of the resin, clearance will be easier. With only entry and exit ports at either end for the mass to escape, this would make it harder to clear a long, spiral channel. But as long as clearance occurs, CNFs can no doubt be populated and a wiring matrix achieved.

Once bacteria testing is complete, the next stage is to electrically connect multiple chips to create a power cube. The results from the 30-60 day experiments should provide a baseline for the expected power generation of a single chip. The expected power of a cube consisting of multiple chips can be extrapolated and calculated from this data. Bacteria experiments of

30-60 days would be repeated for this configuration. At this point, the final product would be achieved and the focus would shift to optimization i.e. providing the best environment for the bacteria to thrive via filtering, flow, and food availability.

CHAPTER 5:
Conclusion

The research presented in this thesis has yielded a viable procedure for populating a CNF wiring matrix in a square microchannel. The procedure demonstrates consistent success in square channels between 500 and 1100 microns with achievable resistances as low as 6 kΩ. These results are a critical milestone in designing and manufacturing BMFC power cubes to sustain naval and underwater assets. Providing a method of electrode wiring within an architectural structure is key to providing benthic bacteria an optimum environment for power producing conditions. Optimum power producing conditions will open the door for both unmanned vehicles and sensor networks to greater stealth, longer operating times, farther operating areas, and less reliance on capital ships and contested supply lines.

Engineered BMFC power cubes within this project are not far into the future. The wired channels are currently ready to accept bacteria for loading to undergo power generation trials. When these trials are complete, the power cube stage will commence. The underlying design feature of these chips from the beginning has been to ensure scalability, and this feature has been preserved. Multiple chips will be electrically connected as a single unit and prepared to undergo further biological testing. This final product stage likely requires a year or less to realize, depending on manpower provided to the project.

The U.S. Navy's capabilities will undoubtedly rise with the introduction of reliable remote power in various domains. Clandestine charging stations to maintain tactical control, facilitate longer deployed operating times, increase instrument longevity and capability, lower costs and maintenance requirements, and lessen dependence on capital ships are only some of the advantages this technology will provide. Remote power via renewable energy is increasingly important in a time where climate change exists in force, along with a concerted effort to wean off reliance on foreign resources. Additionally, the U.S. Navy continues to increase operations abroad to support freedom of navigation and respond to the changing global political climate. After all, the Navy operates almost exclusively abroad because it is the frontline deterrent to ensuring conflict does not reach domestic shores. BMFC technology could be a key asset in supporting these deployed missions in the future.

THIS PAGE INTENTIONALLY LEFT BLANK

List of References

[1] *Report to Congress on the Annual Long-Range Plan for Construction of Naval Vessels for Fiscal Year 2023*, Office of the Chief of Naval Operations, Washington, DC, USA, Apr. 2022. [Online]. Available: https://media.defense.gov/2022/Apr/20/2002980535/-1/-1/0/PB23%20SHIPBUILDING%20PLAN%2018%20APR%202022%20FINAL.PDF.

[2] *Chief of Naval Operations Navigation Plan 2022*, 2022. [Online]. Available: https://www.dvidshub.net/publication/issues/64582.

[3] *Department of the Navy Climate Action 2030*, May 2022. [Online]. Available: https://www.navy.mil/Portals/1/Documents/Department%20of%20the%20Navy%20Climate%20Action%202030.pdf.

[4] L. M. Tender, "Microbial fuel cells for powering Navy devices," Naval Research Laboratory, Washington, DC, USA, Tech. Rep., 2014. [Online]. Available: https://apps.dtic.mil/sti/pdfs/ADA594746.pdf.

[5] Y. M. Arias, T. Lewis-Hsu, K. Richter, and D. B. Chadwick, "Transition applications for benthic microbial fuel cells," en, SPAWAR, San Diego, CA, USA, Tech. Rep., 2016. DOI: 10.13140/RG.2.2.31810.48326. [Online]. Available: https://www.researchgate.net/publication/318085479_Transition_Applications_for_Benthic_Microbial_Fuel_Cells.

[6] D. Lal, "Microbes to generate electricity," *Indian Journal of Microbiology*, vol. 53, no. 1, pp. 120–122, Jan. 2013. DOI: 10.1007/s12088-012-0343-2. [Online]. Available: https://www.ncbi.nlm.nih.gov/pmc/articles/PMC3587501/.

[7] D. R. Lovley, "Bug juice: Harvesting electricity with microorganisms," *Nature Reviews Microbiology*, vol. 4, no. 7, pp. 497–508, Jul. 2006. DOI: 10.1038/nrmicro1442.

[8] B. E. Logan and J. M. Regan, "Electricity-producing bacterial communities in microbial fuel cells," *Trends in Microbiology*, vol. 14, no. 12, pp. 512–518, Dec. 2006. DOI: 10.1016/j.tim.2006.10.003.

[9] M. E. Nielsen, C. E. Reimers, and H. A. Stecher, "Enhanced power from chambered benthic microbial fuel cells," *Environmental Science and Technology*, vol. 41, no. 22, pp. 7895–7900, Oct. 2007. DOI: 10.1021/es071740b.

[10] B. E. Logan, *Microbial Fuel Cells*, 1st ed. Hoboken, New Jersey: John Wiley Sons, Incorporated, Jan. 2008. [Online]. Available: http://ebookcentral.proquest.com/lib/ebook-nps/detail.action?docID=331621.

[11] A. Zabihallahpoor, M. Rahimnejad, and F. Talebnia, "Sediment microbial fuel cells as a new source of renewable and sustainable energy: Present status and future prospects," *RSC Advances*, vol. 5, no. 114, pp. 94 171–94 183, 2015. DOI: 10.1039/c5ra15279h.

[12] *Department of the Navy 30 year rdt+e 30 year research and development plan (2017);* [Online]. Available: https://www.researchgate.net/figure/Conceptual-Vision-of-the-Operational-Battlespace-of-2045-Source-1_fig1_353298603.

[13] Y. M. Arias-Thode, L. Hsu, G. Anderson, *et al.*, "Demonstration of the SeptiStrand benthic microbial fuel cell powering a magnetometer for ship detection," *Journal of Power Sources*, vol. 356, pp. 419–429, Jul. 2017. DOI: 10.1016/j.jpowsour.2017.03.045.

[14] C. Reimers and M. Wolf, "Power from benthic microbial fuel cells drives autonomous sensors and acoustic modems," *Oceanography*, vol. 31, no. 1, pp. 98–103, Mar. 2018. DOI: 10.5670/oceanog.2018.115.

[15] Y Meriah Arias-Thode, L. Hsu, A. Wotawa-Bergen, and B. Chadwick, "Chitin lengthens power production in a sedimentary microbial fuel cell chitin in sedimentary microbial fuel cell," en, 2013. DOI: 10.13140/2.1.2944.3843.

[16] Y. Gao, M. Mohammadifar, and S. Choi, "From microbial fuel cells to biobatteries: Moving toward on-demand micropower generation for small-scale single-use applications," *Advanced Materials Technologies*, vol. 4, no. 7, p. 1 900 079, Mar. 2019. DOI: 10.1002/admt.201900079.

[17] H. Beyenal, *Biofilms in Bioelectrochemical Systems from Laboratory Practice to Data Interpretation*. Hoboken, New Jersey, USA: John Wiley Sons, Inc., 2015.

[18] B. E. Logan and J. M. Regan, "Microbial fuel cells—challenges and applications," *Environmental Science and Technology*, vol. 40, no. 17, pp. 5172–5180, Sep. 2006. DOI: 10.1021/es0627592.

[19] D. Bose, V. Kandpal, H. Dhawan, P. Vijay, and M. Gopinath, "Energy recovery with microbial fuel cells: Bioremediation and bioelectricity," in *Energy, Environment, and Sustainability*, Springer Singapore, Dec. 2017, pp. 7–33. DOI: 10.1007/978-981-10-7413-4_2.

[20] C. Santoro, C. Arbizzani, B. Erable, and I. Ieropoulos, "Microbial fuel cells: From fundamentals to applications. a review," *Journal of Power Sources*, vol. 356, pp. 225–244, Jul. 2017. DOI: 10.1016/j.jpowsour.2017.03.109.

[21] B. Li, J. Zhou, X. Zhou, *et al.*, "Surface modification of microbial fuel cells anodes: Approaches to practical design," *Electrochimica Acta*, vol. 134, pp. 116–126, Jul. 2014. DOI: 10.1016/j.electacta.2014.04.136.

[22] S. Cheng and B. E. Logan, "Ammonia treatment of carbon cloth anodes to enhance power generation of microbial fuel cells," *Electrochemistry Communications*, vol. 9, no. 3, pp. 492–496, Mar. 2007. DOI: 10.1016/j.elecom.2006.10.023.

[23] S. Cheng and B. E. Logan, "Increasing power generation for scaling up single-chamber air cathode microbial fuel cells," *Bioresource Technology*, vol. 102, no. 6, pp. 4468–4473, Mar. 2011. DOI: 10.1016/j.biortech.2010.12.104.

[24] S. Cheng, H. Liu, and B. E. Logan, "Increased performance of single-chamber microbial fuel cells using an improved cathode structure," *Electrochemistry Communications*, vol. 8, no. 3, pp. 489–494, Mar. 2006. DOI: 10.1016/j.elecom.2006.01.010.

[25] E. Gambino, K. Chandrasekhar, and R. A. Nastro, "SMFC as a tool for the removal of hydrocarbons and metals in the marine environment: A concise research update," *Environmental Science and Pollution Research*, vol. 28, no. 24, pp. 30 436–30 451, Apr. 2021. DOI: 10.1007/s11356-021-13593-3.

[26] R. Nitisoravut, C. N. D. Thanh, and R. Regmi, "Microbial fuel cells: Advances in electrode modifications for improvement of system performance," *International Journal of Green Energy*, vol. 14, no. 8, pp. 712–723, Jun. 2017. DOI: 10.1080/15435075.2017.1326049.

[27] M. E. Nielsen, C. E. Reimers, H. K. White, S. Sharma, and P. R. Girguis, "Sustainable energy from deep ocean cold seeps," *Energy and Environmental Science*, vol. 1, no. 5, p. 584, 2008. DOI: 10.1039/b811899j.

[28] T. D. Nguyen, "Output Power Optimization of Microbial Fuel Cells by Scalable Microfluidic Devices," Naval Postgraduate School; Monterey, CA, M.S. thesis, 2019. [Online]. Available: https://calhoun.nps.edu/handle/10945/64035.

[29] J. A. Kempa, "Proof of Concept for 3-D Printable Geometry of Microfluidic Benthic Microbial Fuel Cell Device (MBFMC) With Self-Assembled Wiring," Naval Postgraduate School, Monterey, CA, USA, M.S. thesis, 2022. [Online]. Available: https://calhoun.nps.edu/handle/10945/71488.

[30] A. Lekawa-Raus, J. Patmore, L. Kurzepa, J. Bulmer, and K. Koziol, "Electrical properties of carbon nanotube based fibers and their future use in electrical wiring," *Advanced Functional Materials*, vol. 24, no. 24, pp. 3661–3682, Mar. 2014. DOI: 10.1002/adfm.201303716.

[31] Y. Wang and G. J. Weng, "Electrical conductivity of carbon nanotube- and graphene-based nanocomposites," in *Micromechanics and Nanomechanics of Composite Solids*, Springer International Publishing, Jul. 2017, pp. 123–156. DOI: 10.1007/978-3-319-52794-9_4.

Initial Distribution List

1. Defense Technical Information Center
   Ft. Belvoir, Virginia
2. Dudley Knox Library
   Naval Postgraduate School
   Monterey, California